ERDC/GSL SR-09-4

US Army Corps
of Engineers®
Engineer Research and
Development Center

Cavity Expansion Experiments with Spherical Explosive Charges in Concrete

James K. Gran, John Q. Ehrgott, Jr., and J. Donald Cargile

September 2009

Geotechnical and Structures Laboratory

ERDC/GSL SR-09-4
September 2009

Cavity Expansion Experiments with Spherical Explosive Charges in Concrete

James K. Gran

SRI International
333 Ravenswood Avenue
Menlo Park, CA 94025

John Q. Ehrgott, Jr., and J. Donald Cargile

Geotechnical and Structures Laboratory
U.S. Army Engineer Research and Development Center
3909 Halls Ferry Road
Vicksburg, MS 39180-6199

Final report

Prepared for Defense Threat Reduction Agency
DTRA/CXSS
8725 John J. Kingman Road
Fort Belvoir, VA 22060-6201

Under W912HZ-08-P-0015

Monitored by Geotechnical and Structures Laboratory
U.S. Army Engineer Research and Development Center
3909 Halls Ferry Road, Vicksburg, MS 39180-6199

Abstract: Three experiments were conducted with 1-lb explosive spheres embedded in large concrete cylinders with flatpack stress gages and Dremin loop velocity gages surrounding the charge. In two tests, the charge was far from the boundaries and was fully contained. Radial stresses and velocities attenuated with range by approximately $1/r^{2.5}$. In the third test the charge was near the top surface of the concrete cylinder, and reflections perturbed the sphericity of the flow.

Contents

Figures and Tables

Figures

Tables

Preface

The work described herein was performed by staff members of SRI International (SRI) for the U.S. Army Engineer Research and Development Center (ERDC) under Contract No. W912HZ-08-P-0095. This work was funded by the Defense Threat Reduction Agency (DTRA), Weapon Effects and Planning Tools Branch (CXSS). LTC Henry F. Marcinowski III was the CXSS Program Manager.

Dr. James K. Gran, SRI, was Principal Investigator for this contract research effort. The ERDC Contracting Officer's Representative for this effort was Dr. J. Donald Cargile, Geotechnical and Structures Laboratory (GSL), Engineering Systems and Materials Division.

The ERDC experiment Principal Investigators were John Q. Ehrgott, Jr., and Michael D. Guillet, Impact and Explosion Effects Branch (IEEB), GSL. IEEB engineering technicians assisted in the conduct of the experiment. Placement of the concrete was overseen by personnel of the GSL Concrete and Materials Branch (CMB). The report was prepared by Dr. Gran, Mr. Ehrgott, and Dr. Cargile.

During preparation of this report, Henry S. McDevitt, Jr., was Chief, IEEB; Toney K. Cummins was Chief, CMB; Dr. Larry N. Lynch, was Chief, ESMD, Dr. William P. Grogan was Deputy Director, GSL, and Dr. David W. Pittman was Director, GSL.

COL Gary E. Johnston was Commander and Executive Director of ERDC. Dr. James R. Houston was Director.

Summary

The primary objective of these tests was to support the development of computational models for penetration and explosions in concrete by measuring the stresses and motions near a rapidly expanding cavity. The secondary objective of these tests was to validate the accuracy of low-cost stress gages (carbon and PVDF flatpacks) developed in a recent project (Rickman et al. 2006) by comparing their performance with the measurements from SRI ytterbium flatpack stress gages for which accuracy has been demonstrated over several decades of use.

The conceptual design of these cavity expansion tests is detonation of a 1-lb spherical explosive charge embedded in WES5000 concrete with both flatpack stress gages and Dremin loop velocity gages placed at several radial distances from the charge and oriented to measure the radial component of stress and motion. In the first two tests, the charge was fully contained by the concrete specimen, and the reflections from the boundaries arrived at the gages after the peak displacements were achieved. In the third test, the charge was placed nearer a flat free surface, and the measurements illustrated the effect of the free surface.

In general, these tests were very successful. All the ytterbium flatpack stress gages and all the Dremin loops functioned very well and provided excellent data. The results were very repeatable with the exception that the wave front measured by the Dremin loops in Test 2 appeared to have been dispersed very near the charge. The effect of the free surface near the charge in Test 3 was clearly captured in the velocity measurements. Thus, the data goals were accomplished.

Figure S1a shows all the ytterbium flatpack stress records from the two fully contained tests. Figure S1b shows the Dremin loop velocity records from the two arrays in the first test. The wave profiles have an elastic precursor traveling at a speed of about 4300 m/s and a plastic wave traveling at about 3200 m/s. Peak stress attenuation with range and peak velocity attenuation with range are plotted in Figure S2.

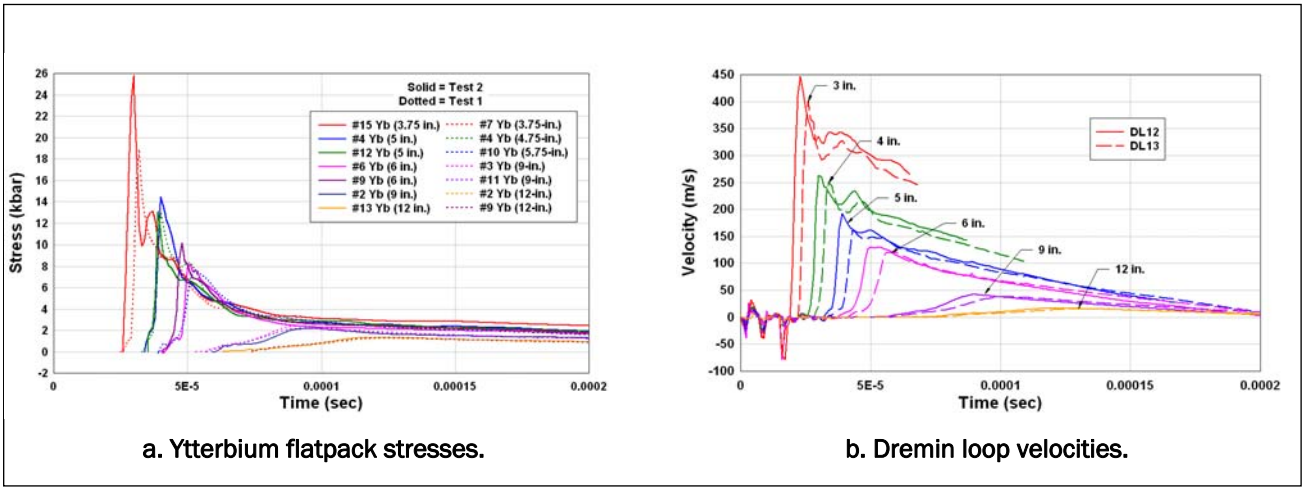

a. Ytterbium flatpack stresses. b. Dremin loop velocities.

Figure S1. Spherical wave stress and velocity time-history measurements.

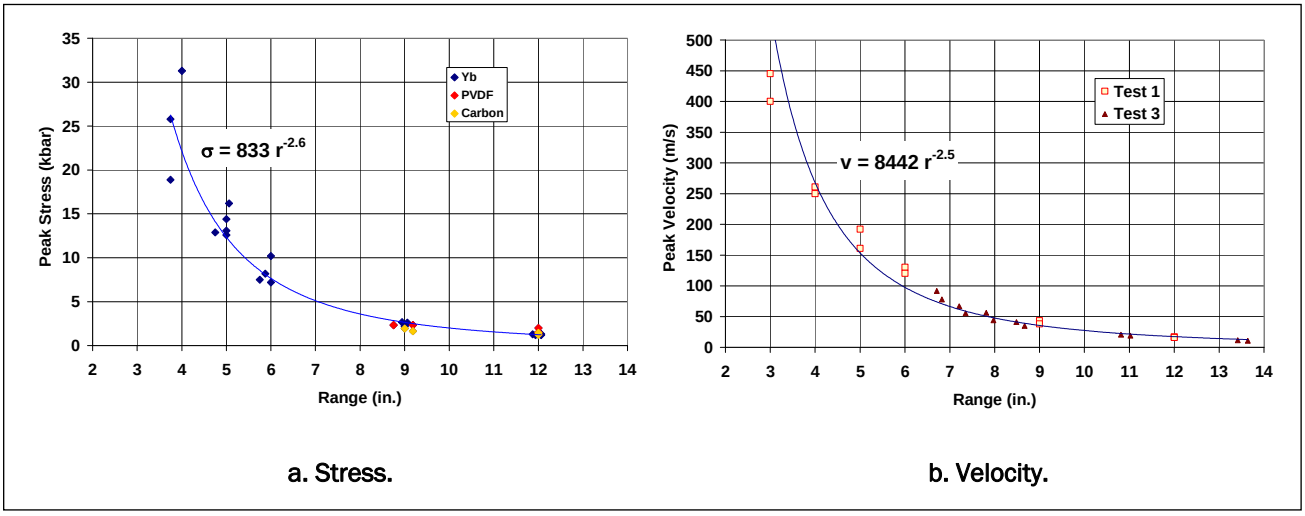

a. Stress. b. Velocity.

Figure S2. Spherical wave attenuation with range.

The performance of carbon and PVDF flatpack gages was mixed. The results from them agreed fairly well with the ytterbium flatpacks at the same ranges, but there was more scatter and two clear outliers. Also, the data from one of the carbon flatpacks and from two of the PVDF flatpacks could not be used at all because of the electromagnetic noise. The stress records from the carbon and PVDF flatpacks are compared with the ytterbium stresses in Figure S3.

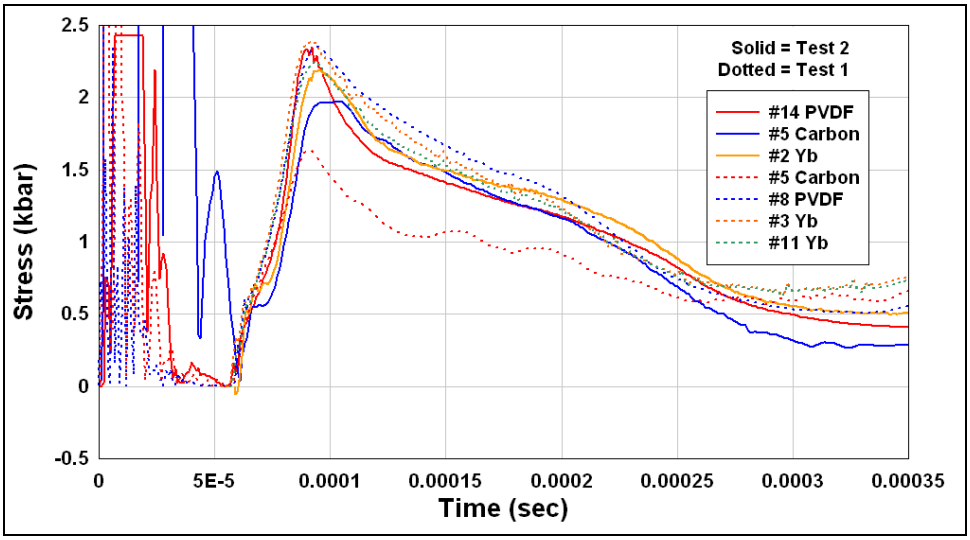

a. 9-in. radius.

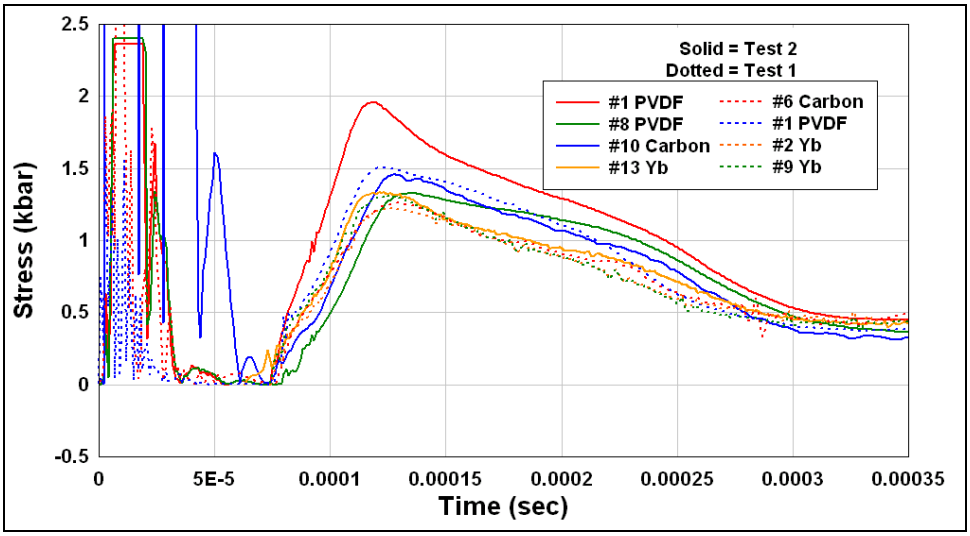

b. 12-in. radius.

Figure S3. Performance of carbon and PVDF flatpack stress gages compared with ytterbium flatpack stress gages.

1 Introduction

The primary objective of these tests was to support the development of computational models for penetration and explosions in concrete by measuring the stresses and motions near a rapidly expanding cavity. The stresses computed to act on the nose of a penetrator by both high-fidelity models (such as EPIC) and fast-running models (such as PENCRV) depend on the high-pressure and high rate of deformation response of concrete in divergent flow. The divergent strain paths of interest are not reproduced in plate-impact experiments, the high pressures of interest are not produced in Hopkinson-bar dynamic experiments, and the high rate of deformation of interest is not achievable in triaxial compression or extension tests. Thus, the explosive cavity expansion tests performed in this project provide unique concrete response data.

The secondary objective of these tests was to validate low-cost stress gages (carbon and PVDF flatpacks) developed in a recent project (Rickman et al. 2006) by comparing their performance with the measurements from SRI ytterbium flatpack stress gages for which accuracy has been demonstrated over several decades of use.

The conceptual design of these cavity expansion tests is detonation of a 1-lb spherical explosive charge embedded in WES5000 concrete with both flatpack stress gages and Dremin loop velocity gages placed at several radial distances from the charge and oriented to measure the radial component of stress and motion. In the first two tests, the charge was fully contained by the concrete specimen, and the reflections from the boundaries arrived at the gages after the peak displacements were achieved. In the third test, the charge was placed nearer a flat free surface, and the measurements illustrated the effect of the free surface.

All three tests were performed at the U.S. Army Engineer Research and Development Center (ERDC), Vicksburg, MS, with instrumentation and fielding support provided by SRI International (SRI), Menlo Park, CA. The flatpack stress gages and the Dremin loops were fabricated at SRI and shipped to ERDC for placement. ERDC constructed the targets, including the fixtures for gage positioning, and placed the concrete onsite. The Air Force Research Laboratory (AFRL) at Eglin Air Force Base, FL, provided

the explosive spheres; ERDC placed the charges and provided the timing, firing, and data recording. SRI set up the ytterbium flatpack and Dremin loop instrumentation; ERDC set up the carbon and PVDF flatpacks. All the data were analyzed by SRI.

The plan for future experiments is to take measurements around cavities of other shapes using a conical or ogive-shaped explosive charge, and to measure other components of stress and motion.

2 Test Description and Results

Test description

The conceptual test designs are illustrated in Figure 1. In Tests 1 and 2, all the measurements were made in the equatorial plane of the charge. In Test 3, the stress measurements were also in the equatorial plane, but the velocity measurements were both above and below the equator to sense the effect of the free surface. The diameter of the concrete cylinders was large enough to provide nominally 350 μs of measurement before the reflection from the outer radial surface arrived at the gages. Reflections from the upper free surface in Test 3 arrived earlier than that.

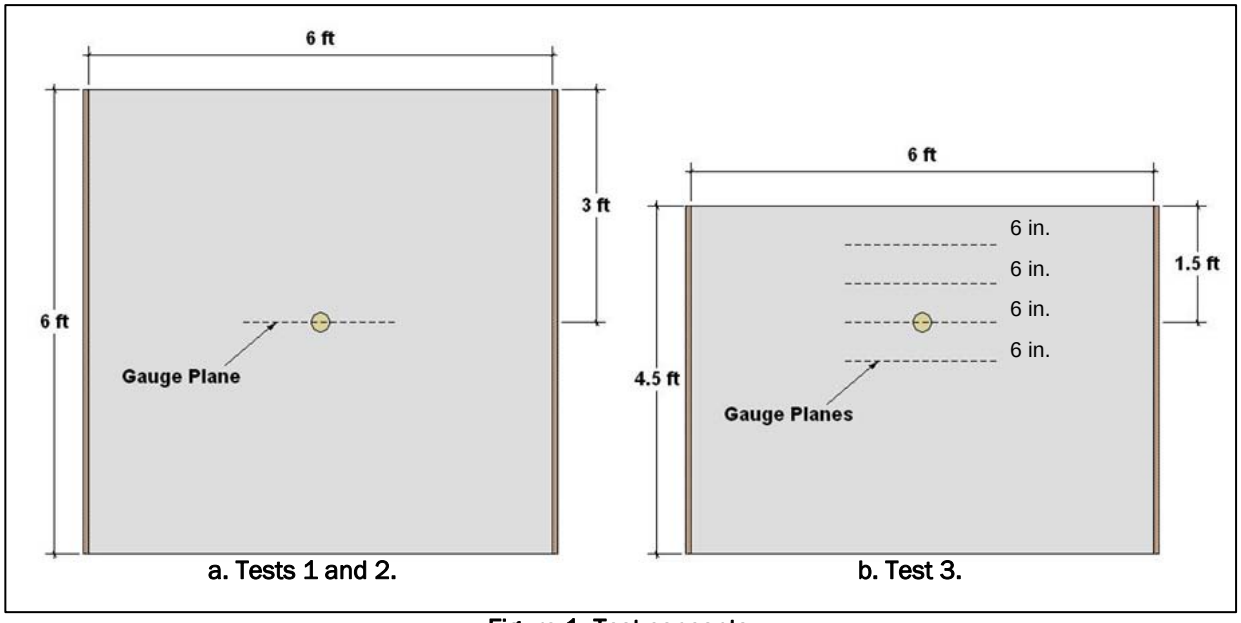

Figure 1. Test concepts.

The design of the ytterbium flatpacks is the same as used in many previous penetration and explosive tests (Gran et al. 1999; 2004) and is illustrated in Figure 2. The sensing element is a 1/2-in. by 1-in. acid-etched grid of 0.002-in.-thick ytterbium foil. It is primarily sensitive to the applied normal stress, but its resistance is also a known function of the in plane stresses and strains applied to it (Chen et al. 1984). The perturbations produced by the in-plane stresses and strains in the ytterbium are eliminated with SRI's PIEZOR analysis using the strain measured by the companion with constantan element (Gran and Seaman 1997). The elements and the

copper foil leads are encapsulated between layers of 0.005-in.-thick Teflon insulation and sandwiched between two strips of 1/16-in.- thick by 2-in.-wide 304 stainless steel, welded together all around the edges. Any space left between the internal layers of the package is filled by pumping epoxy into the end near the elements. The width-to-thickness aspect ratio of the gage and the relatively thin layer of low modulus insulation combine to greatly mitigate the perturbation the gage makes as an inclusion in the concrete. This is even further enhanced by a layer of 0.0005-in.-thick Mylar film on the outside of the steel which decouples the gage and concrete from interface shear stress. The overall length of the flatpack is about 5 ft, long enough to exit the concrete target so that signal cable attachments do not need to be hardened.

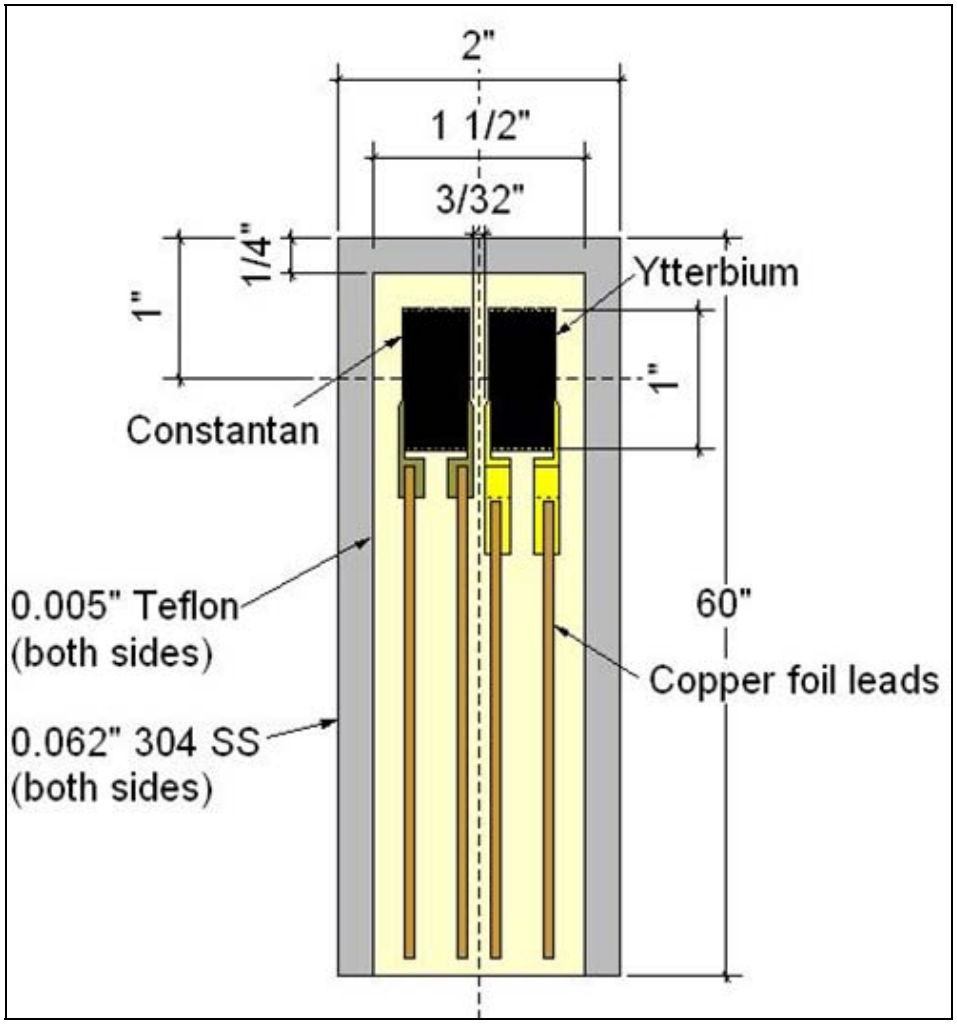

Figure 2. Ytterbium flatpack.

The designs of the carbon and PVDF flatpacks are the same as used in the recent project in which they were developed and originally evaluated with cylindrical explosive charges in concrete (Rickman et al. 2006). These designs are illustrated in Figure 3. In both cases, the encapsulated elements were manufactured by Dynasen, Inc., and the manufacturer's sensitivities were used to convert the recorded data to stress units. Although the vapor-deposited carbon element's resistance is also sensitive to in-plane strain, its sensitivity is not well known, so strain compensation is not yet possible. Nevertheless, a companion constantan element was used along side the carbon to monitor the strain and warn of significant problems. The PVDF element is piezoelectric and not immune to in-plane strain, but the manufacturing process is not compatible with vapor-depositing a companion constantan element, so strain was not monitored in those gages.

The Dremin loop velocity gage is a circular loop of conducting wire embedded in the concrete with a solenoidal magnetic field imposed on the target. The wire moves with the concrete as the stress wave propagates through the target, and the voltage created in the wire is proportional to the velocity of the wire and the strength of the magnetic field. This is illustrated in Figure 4a.

In most past applications, the loops were 360-deg loops concentric with the explosive charge. In this project, the loops were 90-deg segments, also concentric with the charge, so that other quadrants of the concrete target were available for placing the stress gages. The 90-deg segments were made of 0.035-in.-diam copper wire, attached at a few points to a fiberglass grid, as shown in Figure 4(b). The grid was made of 1/8-in.-thick by 1/2-in.-wide strips of fiberglass with shallow notches at the intersections.

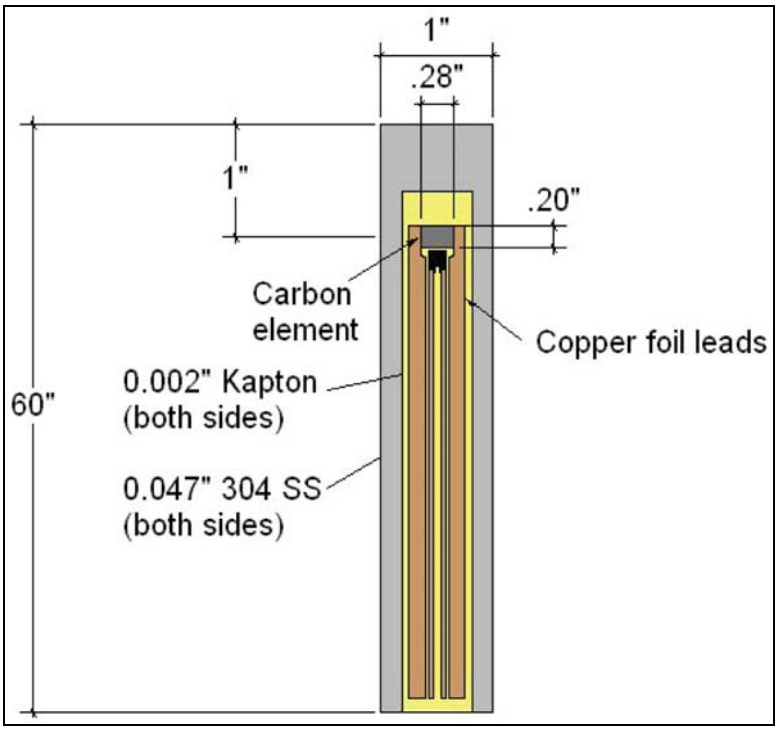

a. Carbon flatpack.

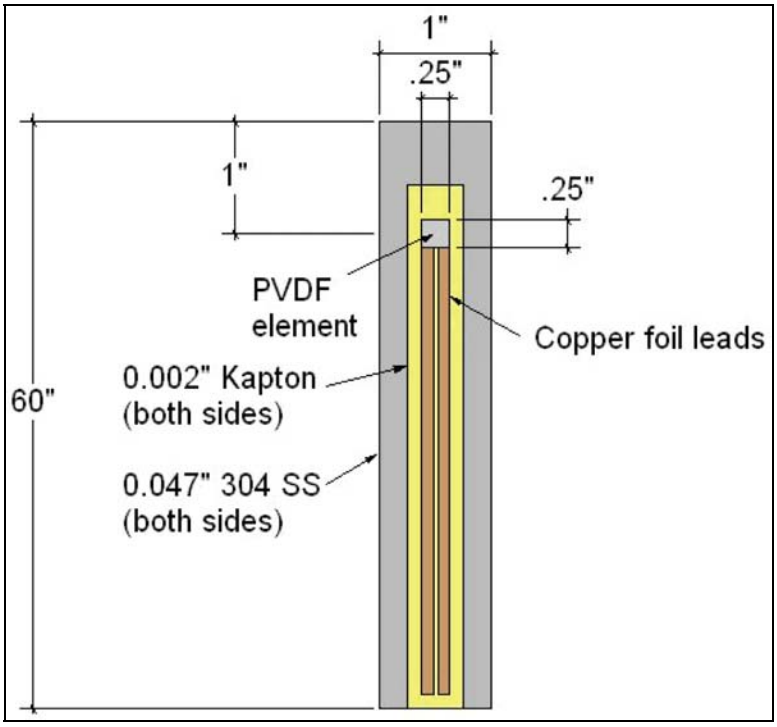

b. PVDF flatpack.

Figure 3. Carbon and PVDF flatpacks.

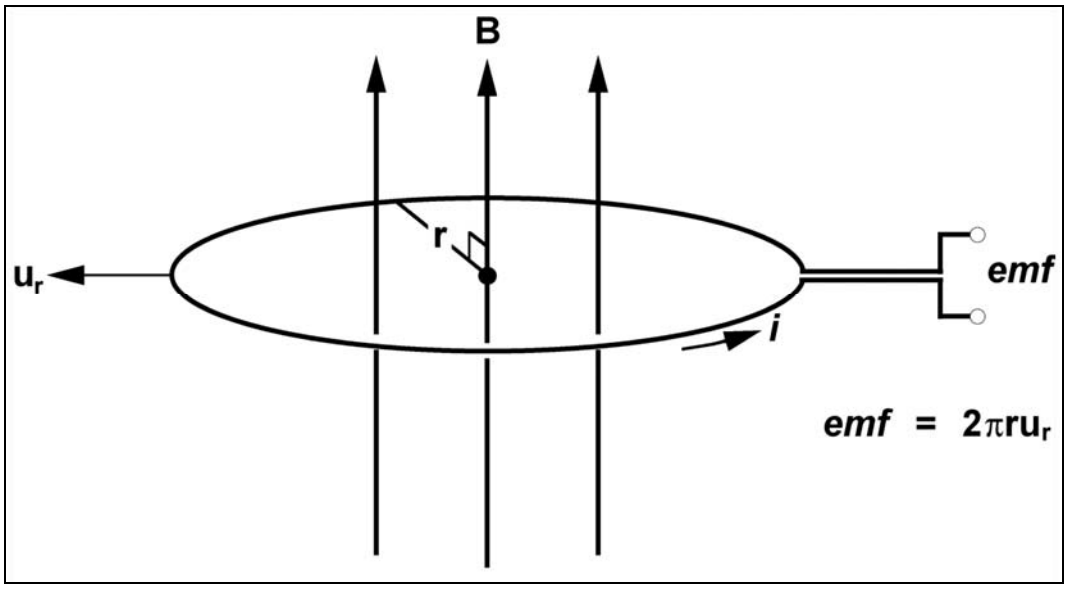

a. Dremin loop principle of operation.

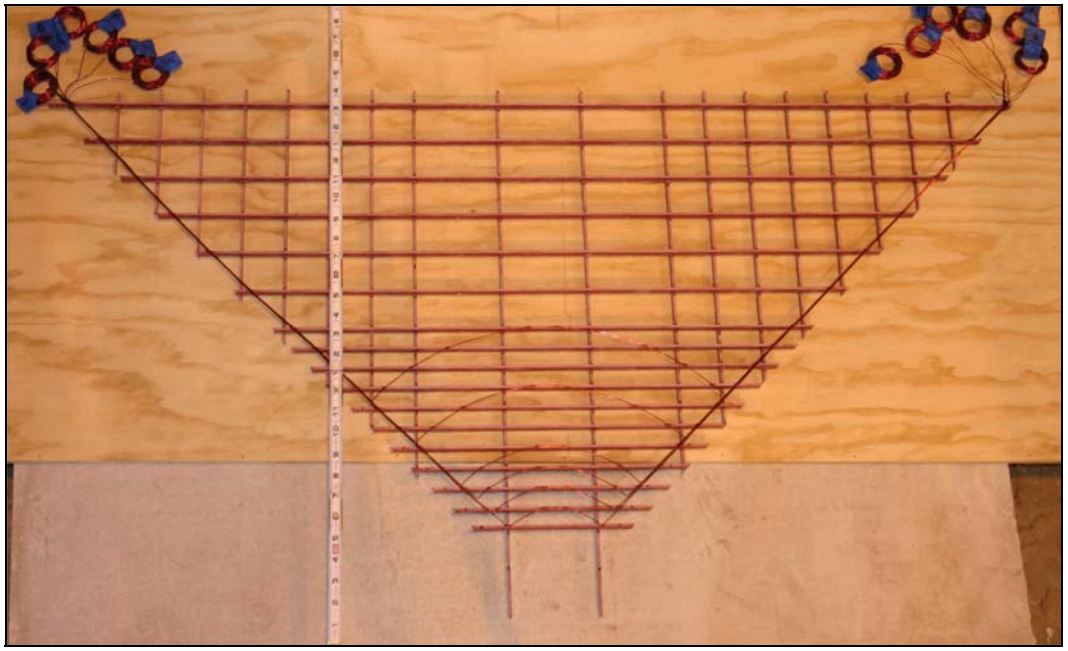

b. 90-deg Dremin loop segments on a fiberglass grid.

Figure 4. Dremin loop segments.

The flatpacks and Dremin loop segments were held in the desired locations and orientations with fixtures inside the concrete formwork. Figure 5 illustrates the target fabrication process. The fixtures were designed to have minimal affect on the stress wave and the gages, mostly by being as far from the explosive charge and the sensing elements as possible. The outer shell was made of fiberglass, so that it would not perturb the magnetic field imposed by external electromagnet (illustrated later).

The WES5000 concrete target material was a conventional mix of Portland cement and natural sand and gravel aggregates with a maximum aggregate size of 3/8 in. The nominal unconfined strength of the concrete is 6000 psi, and the density is about 136 lb/ft^3 (2.18 ± 0.03 g/cm^3). The age of the concrete at the time of the tests was about 60 days.

The explosive spheres were cast Composition B weighing 1.00 ±0.01 lb. Each was placed inside precast cylindrical hole that was backfilled with a relatively quick-setting grout whose properties are a reasonable match to the concrete. The charge was centered in the hole with plastic spacers, and its depth controlled by the length of the brass tube attached. Figure 6 illustrates the placement of a charge. The explosive was initiated at its center with an RP-1 exploding bridge-wire (EBW) detonator. Wires for the detonator ran up the inside of the brass tube.

Figure 7 shows the Test 1 target pretest and posttest. The large ring around the outside of the target is the 7-ft-diam electromagnet for the Dremin loops. In the posttest photograph, the concrete surface cracks were highlighted.

Of the 21 ytterbium flatpacks employed, all returned excellent records. Of the six carbon flatpacks, four provided good records, but one of these four appears to be an outlier (relative to the ytterbium and PVDF gages at the same range). Of the six PVDF flatpacks, five provided good records, but one of these five appears to be an outlier (relative to the ytterbium and carbon gages at the same range). All of the 36 Dremin loop segments provided good records, although the three gages at the 3-in. radius and the three gages at the 4-in. radius failed due to excessive circumferential strain prior to the arrival of the reflection of the stress wave.

a. Gage fixture assembly.

b. Concrete placement.

Figure 5. Target fabrication.

a. Spherical charge with spacers.

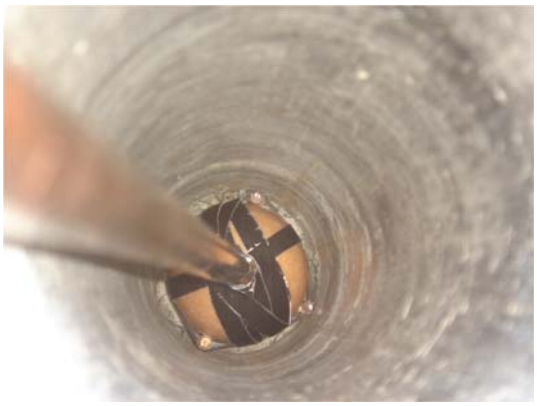

b. Charge in precast hole.

c. Grout backfill.

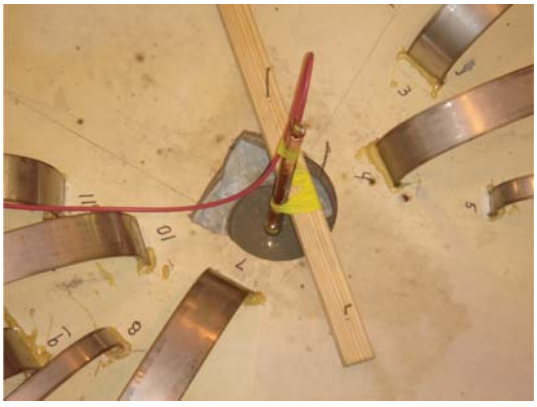

d. Finished installation.

Figure 6. Explosive charge installation.

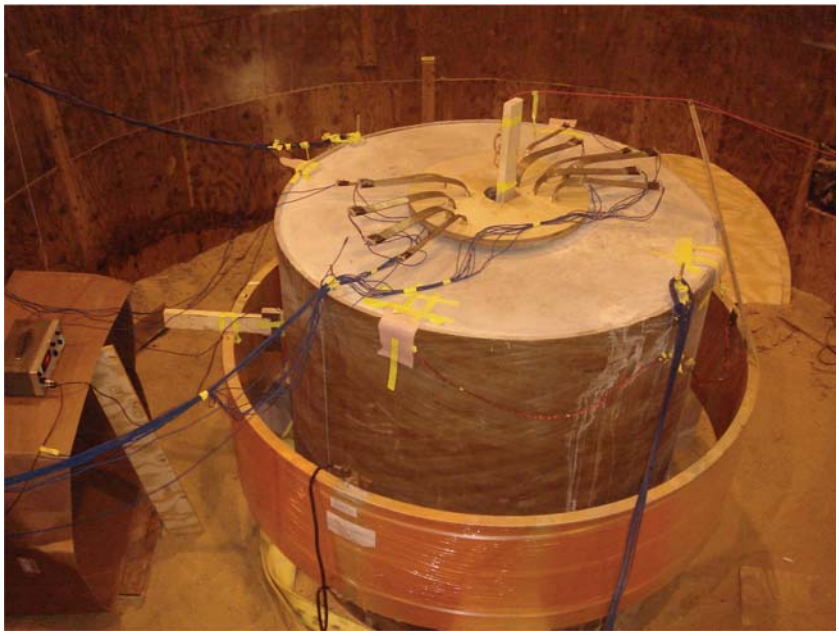

a. Test 1 pretest setup.

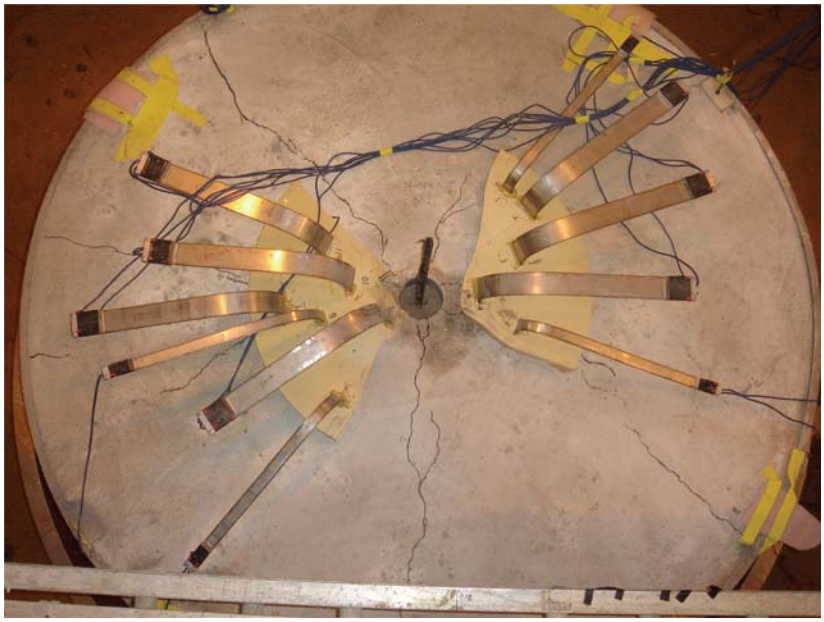

b. Test 1 posttest view.

Figure 7. Pretest and posttest photographs of target from Test 1.

In all three tests, the electromagnetic (EM) noise burst generated by the capacitor discharge to fire the EBW infiltrated the gage signals. This required that the ytterbium and constantan records in the ytterbium flat-packs be truncated prior to the time of arrival (TOA) of the stress wave,

because the PIEZOR analysis would interpret the noise to be spurious strains. It also made the determination of the TOA difficult for the all the gages within 4 in. of the charge center and may have affected the rise and peak signal of some of these gages.

In the next three sections of this report, the data from the three tests are presented; Test 1 and Test 2 are compared, and the effect of the free surface in Test 3 is illustrated. Conclusions and recommendations are offered at the end.

Test 1 results

The layout of the gages in Test 1 is shown in Figure 8, and the as-built locations of the gages are listed in Table 1. The locations of the Dremin loops in the table are the range of the innermost loop. The charge depth is 36 in.

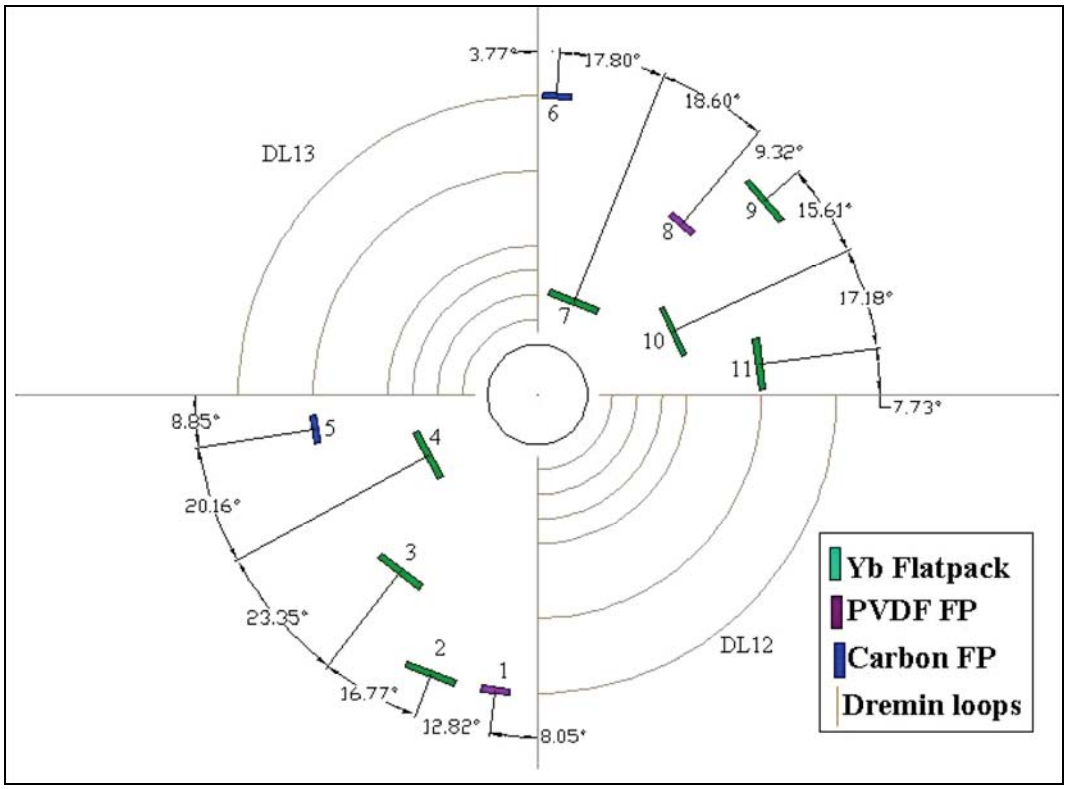

Figure 8. Test 1 gage layout (plane view).

Table 1. Test 1 as-built gage locations (±1/32 in.).

Ref #	Type	Radius	Depth
1	PVDF FP	12 in.	36 in.
2	Yb FP	12.0625 in.	36 in.
3	Yb FP	9 in.	36 in.
4	Yb FP	4.75 in.	36 in.
5	Carbon FP	9.1875 in.	36 in.
6	Carbon FP	12 in.	36 in.
7	Yb FP	3.75 in.	36 in.
8	PVDF FP	9.1875 in.	36 in.
9	Yb FP	11.875 in.	36 in.
10	Yb FP	5.75 in.	36 in.
11	Yb FP	9 in.	36 in.
12	Dremin loops	3 in.	36.0625 in.
13	Dremin loops	3 in.	35.9375 in.

The normal stresses measured by the ytterbium flatpacks are plotted in Figure 9, and the in-plane strains are plotted in Figure 10. All of the gage records have much longer durations than shown here, but reflections from the outer surface of the target arrive at the 12-in radius at about 350 μs. Because the flatpack is thin, and its normal stiffness is high, it registers the applied normal stress with good accuracy. Thus, the stresses plotted in Figure 9 are the radial stresses in the concrete. The Mylar sheathing on the flatpack and the longitudinal stiffness of the flatpack prevent the divergent circumferential strains in the concrete from coupling to the flatpack. Thus, the strains plotted in Figure 10 are the element strains inside the flatpack and are much lower magnitude than the concrete strains at these gage locations (by design). Still, the strains are large enough that they affect the signals from the ytterbium elements, so the PIEZOR analysis is required to resolve the stresses, especially at the three closest ranges.

The stress time-histories exhibit what appears to be an elastic precursor of about 1 kbar, although it may be partially masked by the superposed EM noise that was truncated from the front of the records. This precursor is followed by a strong stress wave whose magnitude decreases, and whose rise time increases with propagation distance. Prior to the arrival of reflections from the boundary, the stresses settle to residual values between about 0.5 and 1.5 kbar.

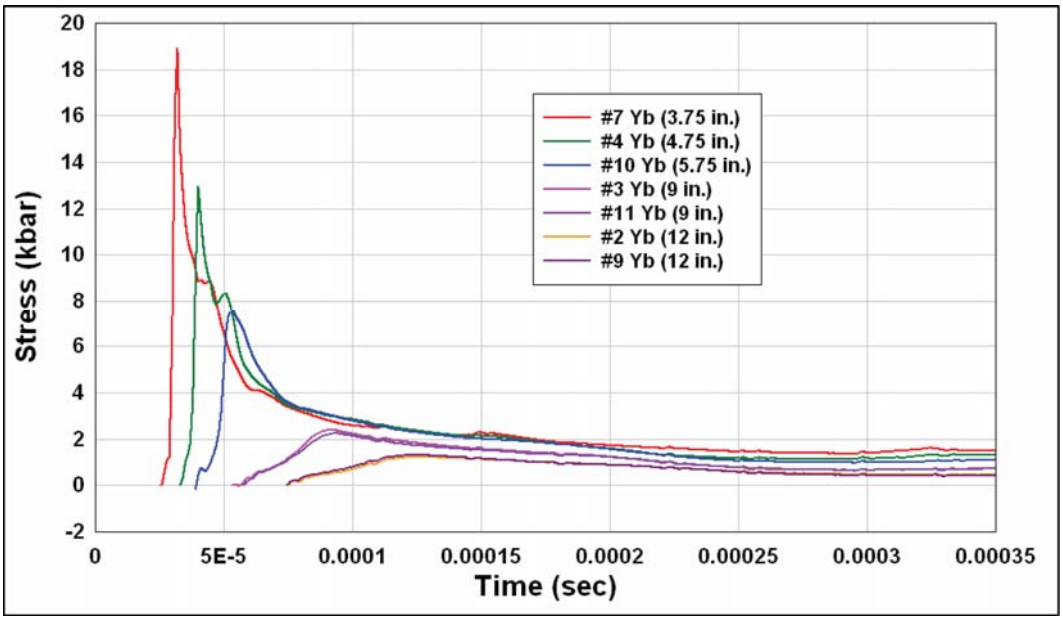

Figure 9. Test 1 ytterbium and constantan normal gage stresses.

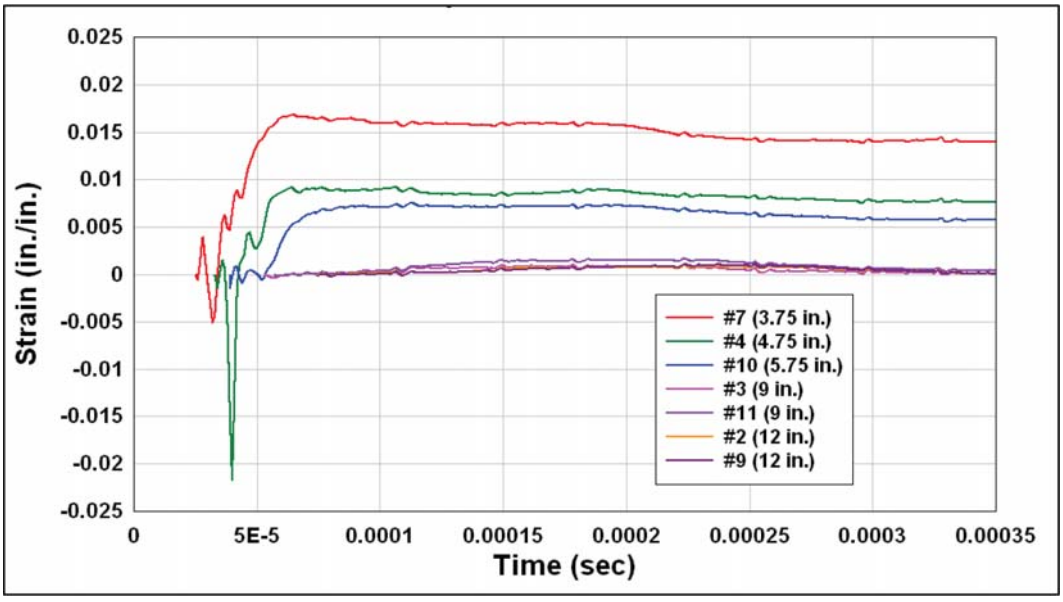

Figure 10. Test 1 ytterbium and constantan in-plane strains.

An expanded-scale plot of the stresses at the 9- and 12-in. radii is shown in Figure 11. The agreement between pairs of gages in different quadrants of the target is excellent. The elastic precursor is still evident at these ranges, although its magnitude has decayed to about 0.5 kbar. The periodic blips in the records are common to all the records and must be due to some other source of noise.

The stresses measured by the carbon and PVDF flatpacks at the 9- and 12-in. radii are plotted in Figures 12 and 13, respectively, along with the ytterbium gage stresses at those ranges. Here the EM noise has not been truncated from the beginning of the records, because the data analysis does not require it, and the plots show that the noise has decayed away by about 40 μs. The carbon and PVDF records have been converted to stress using the Dynasen calibration with no compensation for strain or temperature. The strains measured in the carbon flatpacks with the companion constantan elements are plotted for completeness. The low levels of strain (low record is shown in Figures 12 and 13) suggest that the carbon and PVDF elements were not significantly perturbed by strain.

The PVDF #8 flatpack at the 9-in. radius and the carbon #6 flatpack at the 12-in. radius show excellent agreement with the Yb flatpacks at those radii. However, for uncertain reasons, the other PVDF and carbon flatpacks did not agree with the Yb flatpacks.

The carbon gage at the 9-in. radius (#5) measured a much lower peak than all the other flatpacks at that range. Referring to Figure 8, one might suspect that carbon flatpack #5 was shadowed by Yb flatpack #4, but it must be noted that Yb flatpack #3 would have been similarly shadowed and its stress signal agrees with the others. Thus, we can only speculate that an inhomogeneity in the concrete very near this gage (such as a large void) or a flaw in the gage itself (such as a gap between the steel case and the insulation) caused the low registration. The PVDF #1 flatpack at the 12-in. radius produced a signal about 20% higher than the other gages at that range. It may have been caused by a large aggregate in contact with the gage right at the sensing element—the thinner steel strips used in the carbon and PVDF flatpack are less able to distribute the applied stress evenly. However, this is also only conjecture.

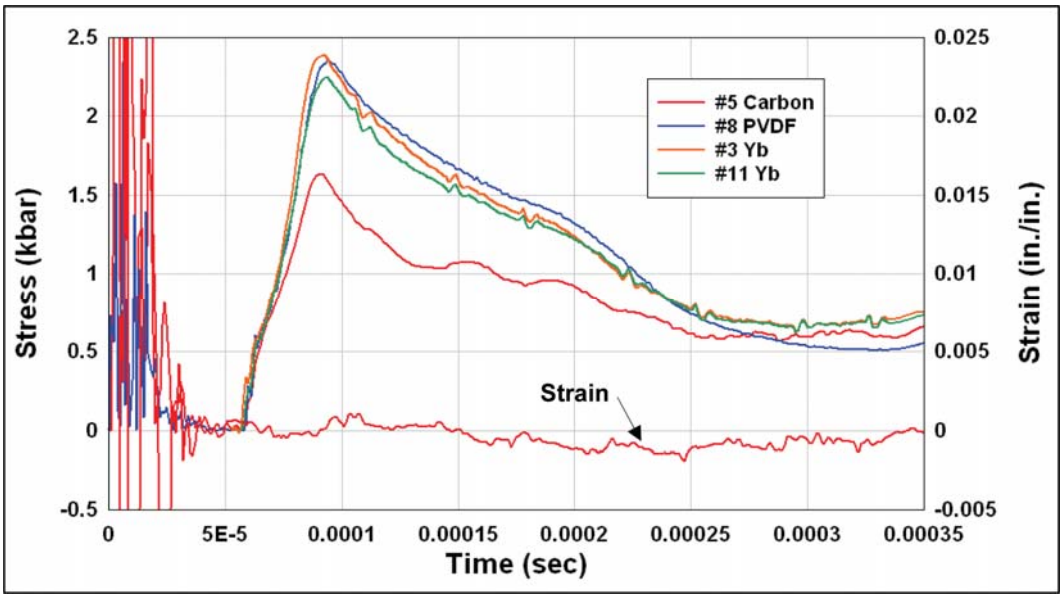

Figure 12. Test 1 carbon and PVDF flatpack stresses at the 9-in. radius.

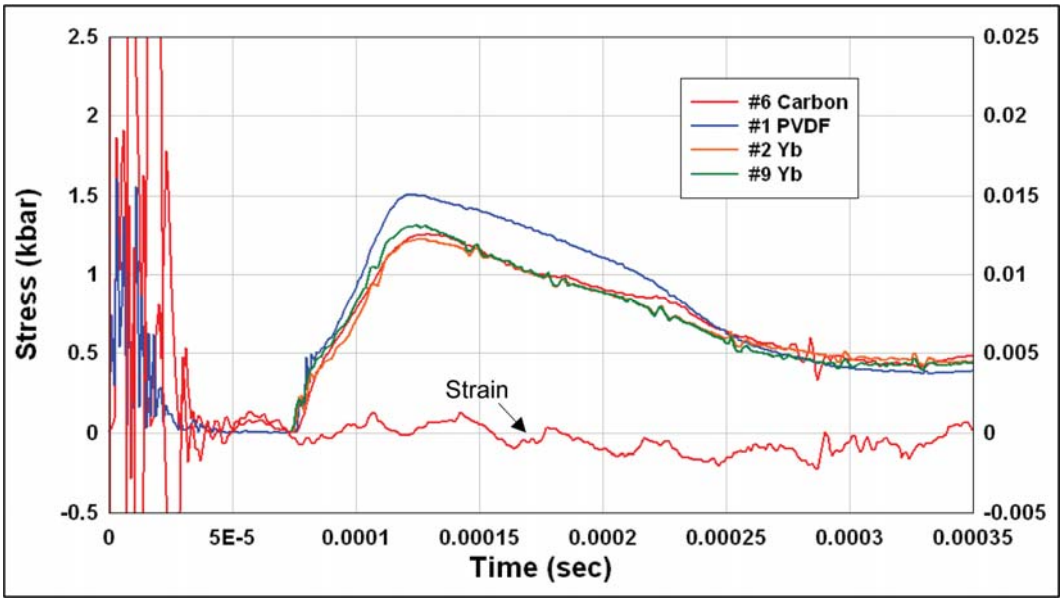

Figure 13. Test 1 carbon and PVDF flatpack stresses at the 12-in. radius.

A check on the accuracy of the stress measurements is provided by a comparison with the measurements made in a previous project (Gran et al. 2004) in which a 1-lb sphere of C-4 explosive was detonated in a large cylinder of similar strength concrete. A plot of peak stress vs. range from that experiment and from Test 1 in this project is presented in Figure 14. The exponents in the power-law fits to the two independent sets of data differ by only about 2.5% from the mean.

Both sets of Dremin loops produced very good measurements of particle velocity at all seven ranges. Plots are shown in Figures 15 and 16. Although the loops at the 3- and 4-in. radii failed in tension, they all survived long after the time of peak velocity. As with the stress records, an elastic precursor is noticeable, particularly at the 5- and 6-in. ranges. The negative phase of the flow was essentially complete by 350 μs. The displacements shown in the plots (dashed lines) are simply numerical integrations of the velocity histories.

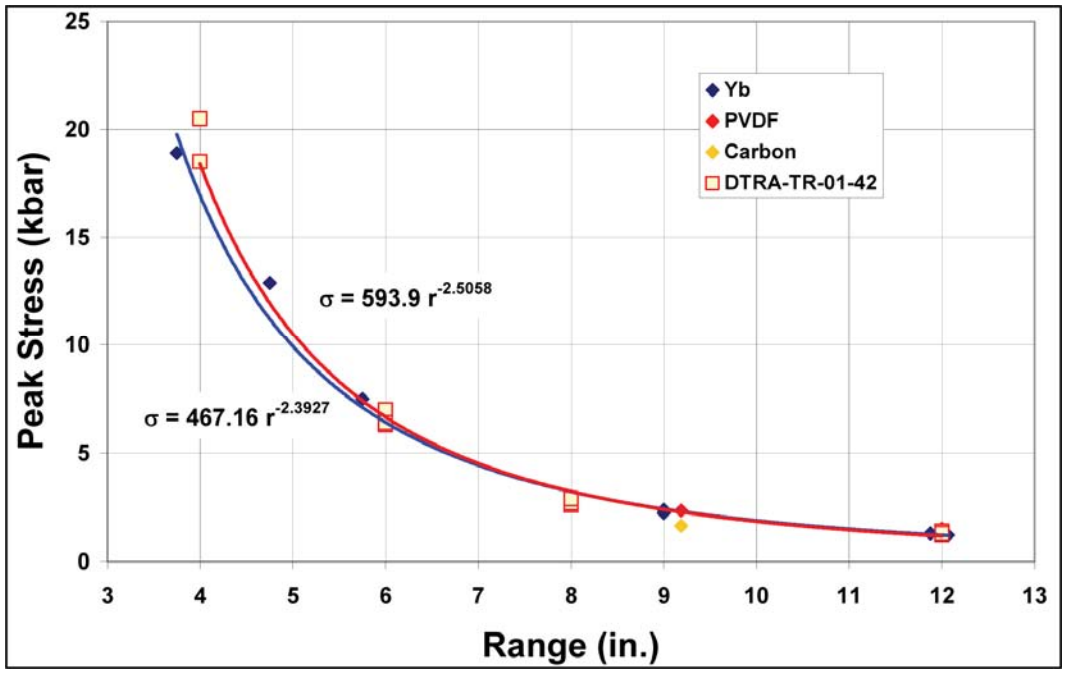

Figure 14. Test 1 peak stress attenuation compared with archive data.

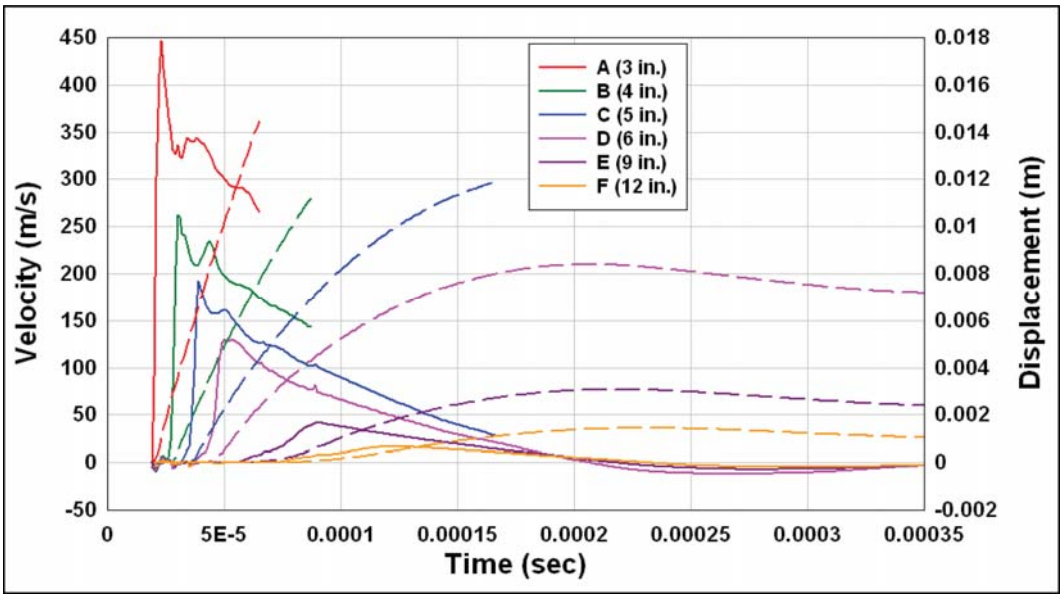

Figure 15. Test 1 Dremin loop radial velocity histories (DL12).

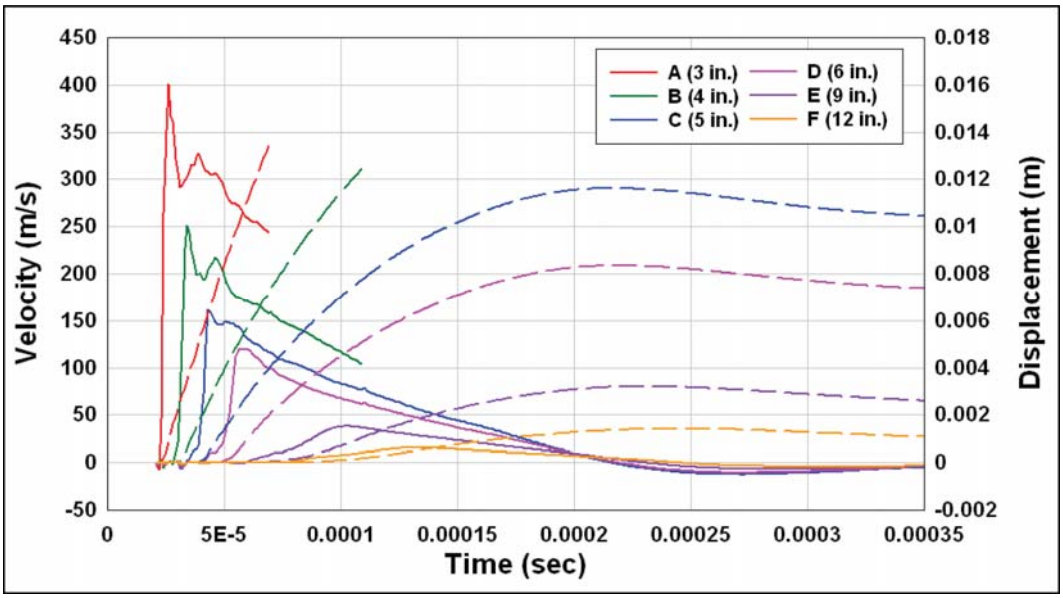

Figure 16. Test 1 Dremin loop radial velocity histories (DL13).

Direct comparisons of the two sets of velocity histories are provided in Figure 17. In general, they compare very well, but the TOAs in the DL13 quadrant are 4 to 6 μs later than in the DL12 quadrant.

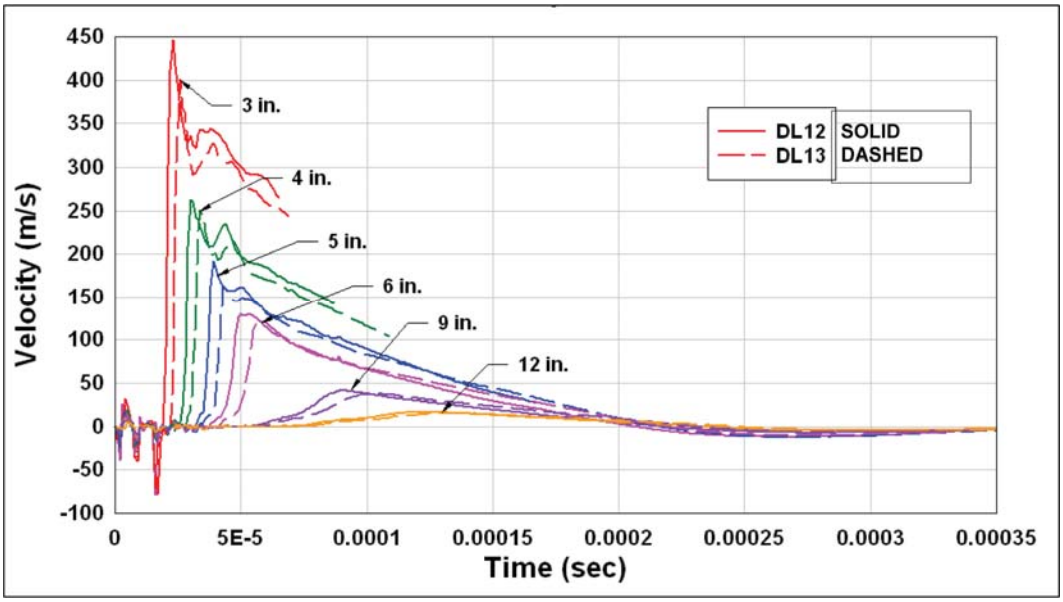

Figure 17. Test 1 Dremin loop velocity history comparison.

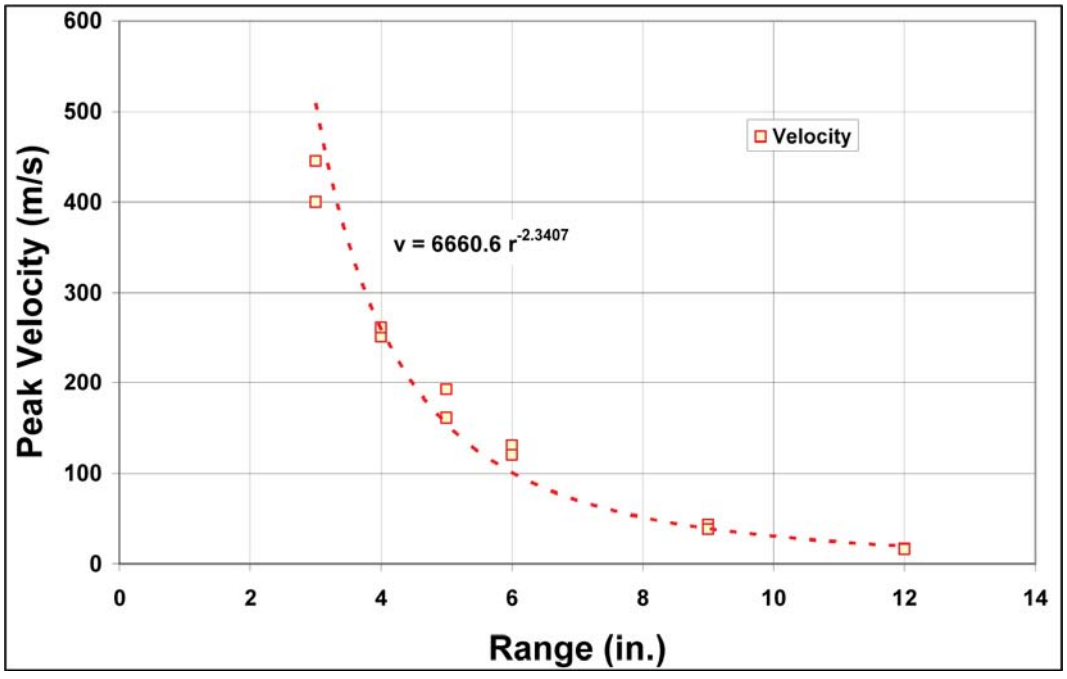

Figure 18. Test 1 velocity attenuation.

The attenuation of the peak velocity with range is shown in Figure 18. The exponent of the power-law fit is almost the same as that for the peak stresses (Figure 14).

The radial displacement histories for the two sets of Dremin loops are compared in Figure 19.

The radial displacements were converted to circumferential strains by dividing by the initial radii for each range. These strains are plotted in Figure 20. The loops at the 3-in. radius strained to nearly 20% before failing.

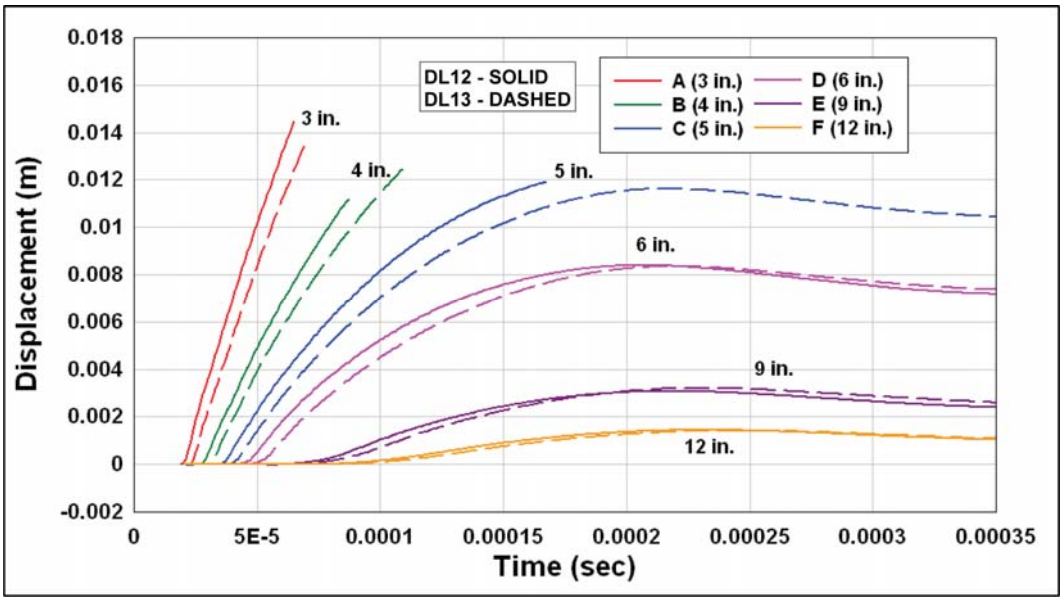

Figure 19. Test 1 Dremin loop displacement history comparison (solid DL12 and dashed DL13).

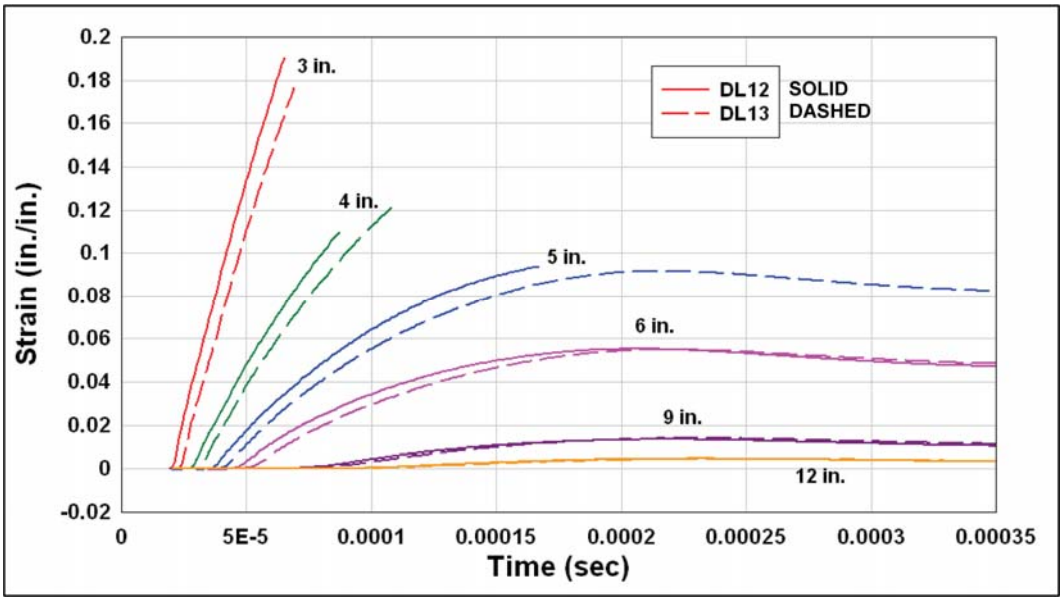

Figure 20. Test 1 circumferential strain histories (solid DL12 and dashed DL13).

Times of first arrival from all of the flatpacks and all the Dremin loops are plotted in Figure 21. The uncertainty bars on the range data are ± ⅛ in., which is much greater than the 1/32-in. uncertainty in the as-built gage locations but potentially true if gages moved during the placement of the concrete. The uncertainty shown for the TOA values is ±1 μs which arises primarily from baseline noise in the records. The straight-line fits to these points indicate a wave velocity of about 4300 m/s for the flatpacks and 4340 m/s for the Dremin loops. These are about 10% higher than the wave speed observed in the previous test in concrete (Gran et al. 2004) for stresses in the same range. Also plotted are the times of arrival of the "plastic wave," that is, the foot of the main pulse following the elastic precursor in the Dremin loop records. These points have more uncertainty (±2 μs) due to the relatively poorer definition of the precursor. In fact, the precursor could not be defined well enough in some records to establish the TOA of the plastic wave. Still, these data are fit fairly well with a straight line that corresponds to a plastic wave velocity c_p of 2960 m/s.

The consistency of the stress and velocity data sets was assessed by applying conservation of momentum to the peak velocity values with the assumption that the precursor can be ignored. That is, we computed a peak stress for each peak particle velocity from the equation $\sigma_{peak} = \rho c_p v_{peak}$ and plotted these values with the measurements of peak stress from the flatpack stress gages. The computed and measured peaks are compared in Figure 22. Although there is scatter within both the stress and velocity data sets, the power-law fits are essentially identical.

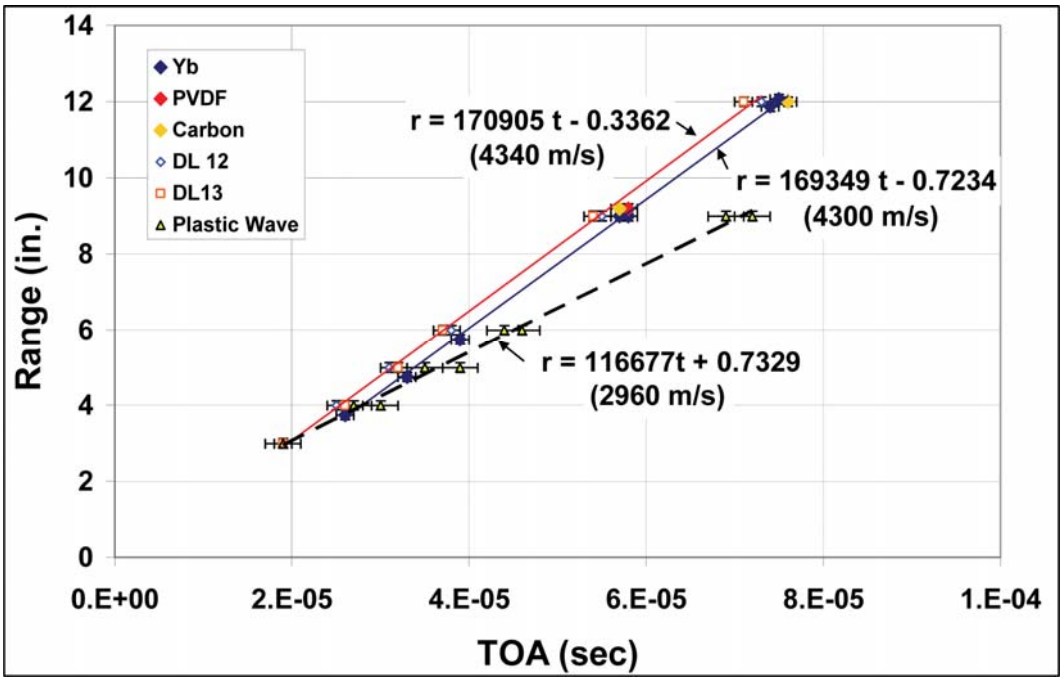

Figure 21. Test 1 times of arrival and wave velocities.

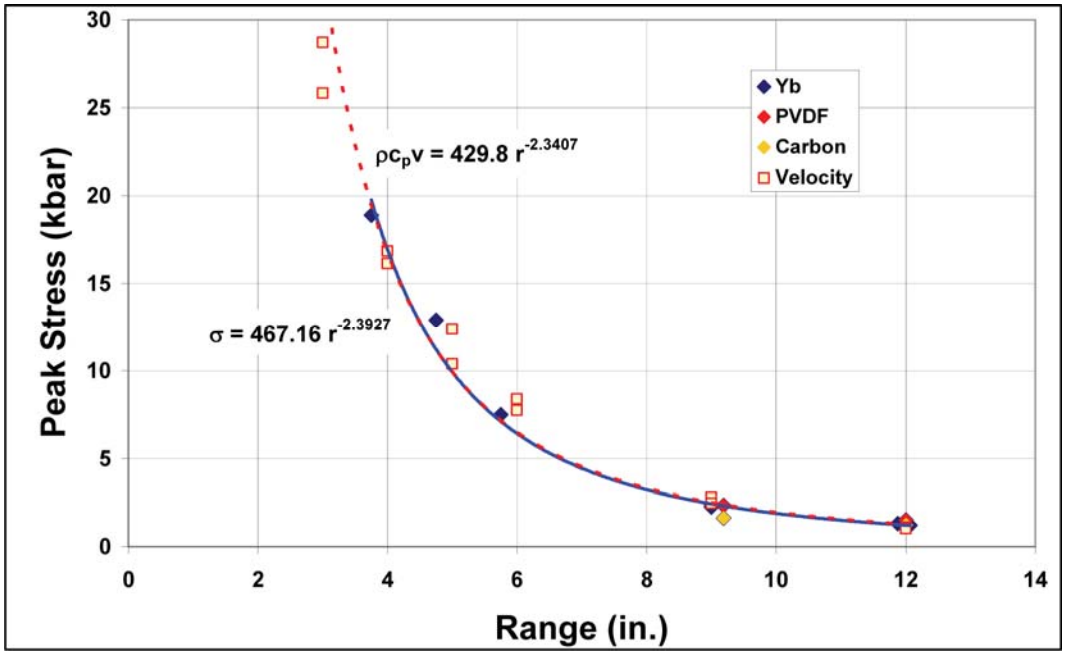

Figure 22. Test 1 peak stress and peak velocity compared.

Test 2 results

The layout of the gages in Test 2 is shown in Figure 23, and the as-built locations of the gages are listed in Table 2. The location of the Dremin loops is the range of the innermost loop. The charge depth is 36 in.

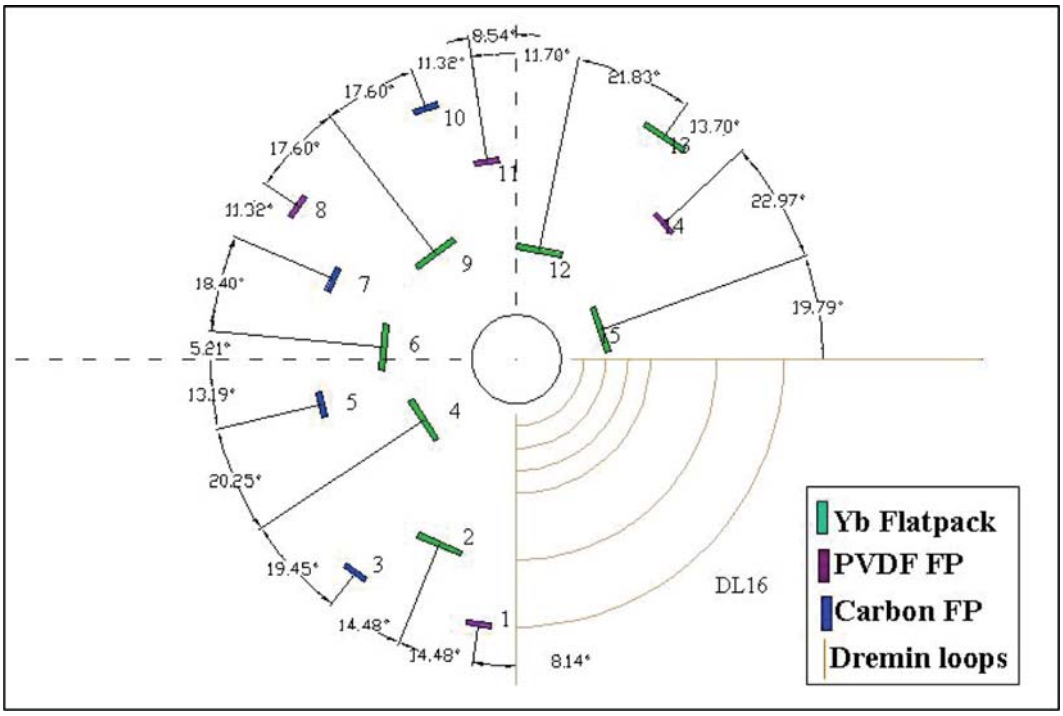

Figure 23. Test 2 gage layout (plan view).

Table 2. Test 2 as-built gage locations (±1/32 in.).

Ref #	Type	Radius	Depth
1	PVDF FP	12 in.	36 in.
2	Yb FP	9 in.	36 in.
3	Carbon FP	12 in.	36 in.
4	Yb FP	5 in.	36 in.
5	Carbon FP	9 in.	36 in.
6	Yb FP	5.875 in.	36 in.
7	Carbon FP	9.125 in.	36 in.
8	PVDF FP	12 in.	36 in.
9	Yb FP	6 in.	36 in.
10	Carbon FP	12 in.	36 in.
11	PVDF FP	9.0625 in.	36 in.
12	Yb FP	5 in.	36 in.
13	Yb FP	12.0625 in.	36 in.
14	PVDF FP	8.75 in.	36 in.
15	Yb FP	3.75 in.	36 in.
16	Dremin loops	3 in.	36.125 in.

The stresses measured by the ytterbium flatpacks are shown in Figure 24, and the in-plane strains in the ytterbium flatpacks are shown in Figure 25. As in Test 1, the records are quite good, but the EM noise from the capacitor discharge again had to be truncated from the front of the signals in order to process them with the PIEZOR analysis.

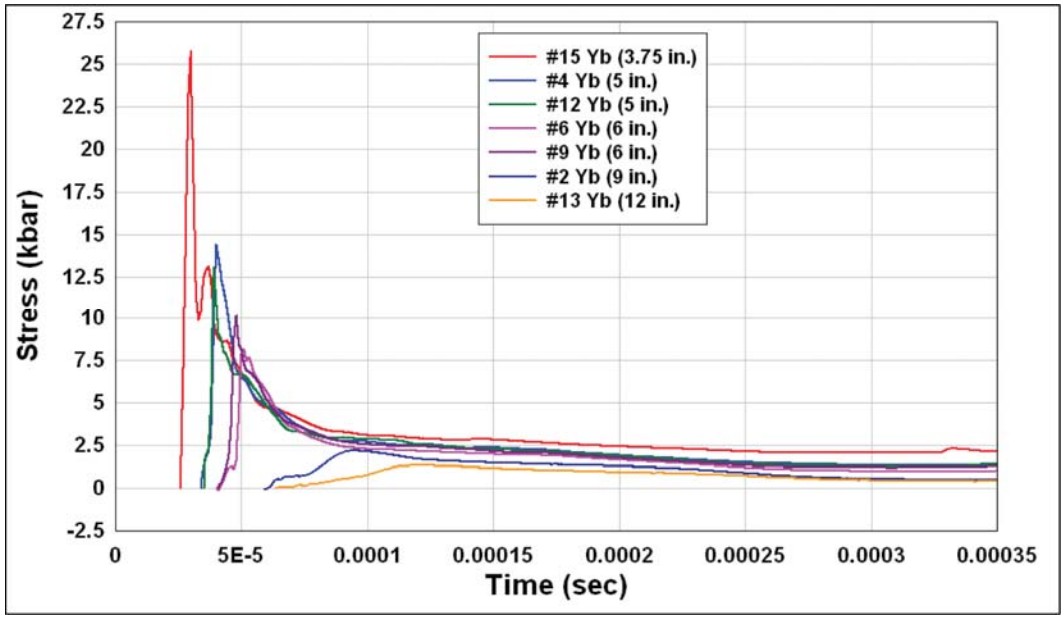

Figure 24. Test 2 ytterbium flatpack stresses.

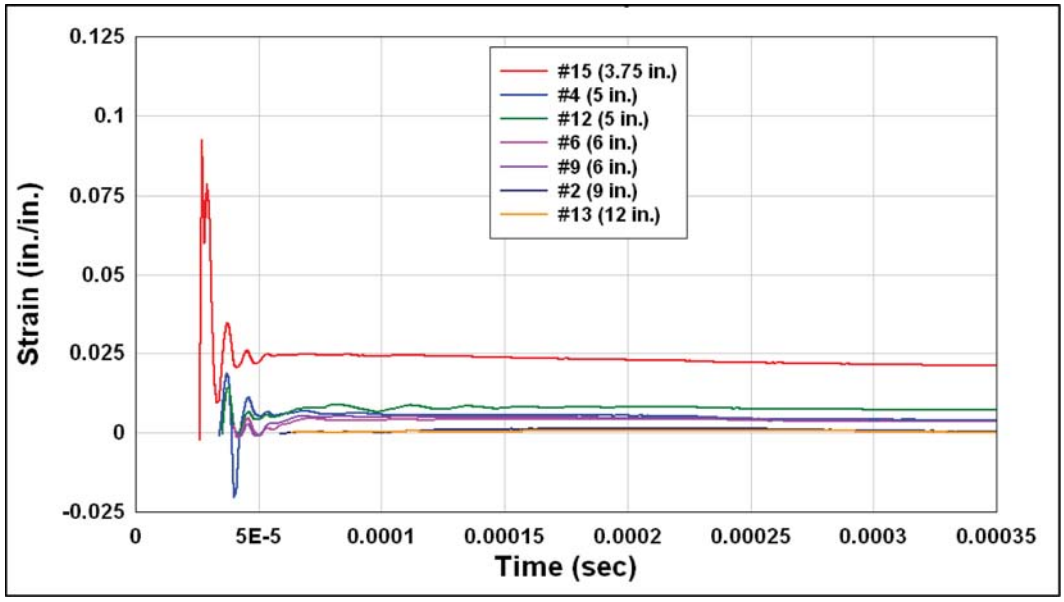

Figure 25. Test 2 ytterbium flatpack strains.

Compared with the Test 1 measurements, the peak stress and peak strain at the closest in gage are higher, but all the rest of the measurements are about the same. Figure 26 plots the stresses from both tests together. The time scale was expanded for clarity and to better illustrate the precursors in the stresses at the nominal ranges of 5 and 6 in.

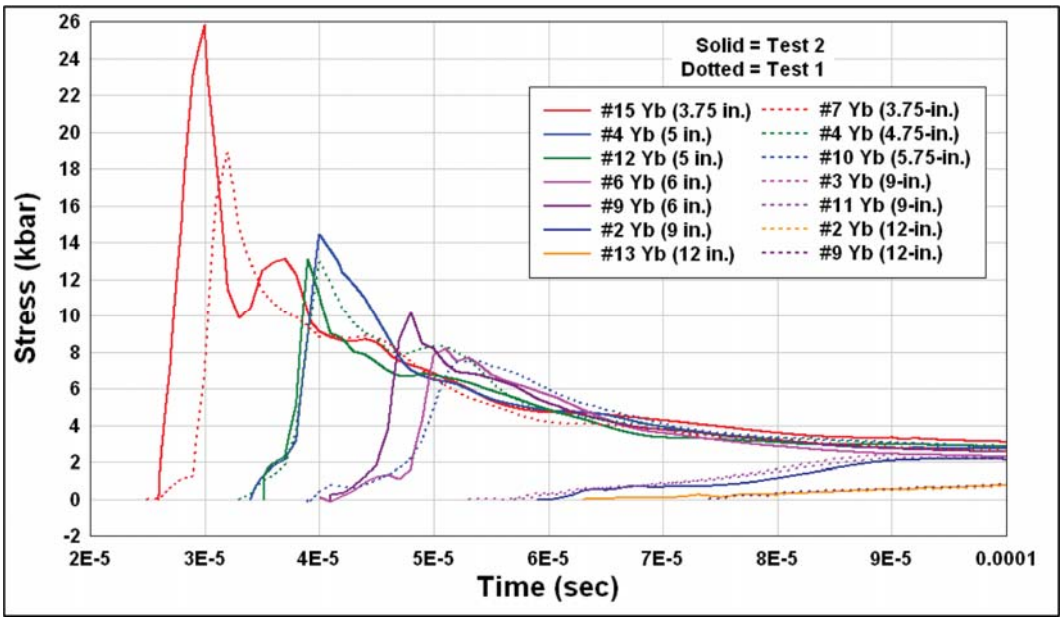

Figure 26. Test 1 and Test 2 ytterbium flatpack stresses compared.

The carbon flatpack and PVDF flatpack stresses at the 9- and 12-in. radii are plotted in Figures 27 and 28. The #5 carbon flatpack at 9 in. in Test 2 registered a slightly lower peak than the five gages that clustered around a peak of about 2.25 kbar, but it otherwise matched the waveforms from those gages. Only the #5 carbon flatpack in Test 1 at this range appears to be an outlier.

The #1 PVDF flatpack in Test 2 at 12 in. registered higher than all the other gages for most of the pulse. As mentioned previously, these differences could be due to gage imperfections or concrete inhomogeneities. Gage strains do not appear to be the problem. However, two carbon flatpacks and one PVDF flatpack in Test 2 provided no useful data, because their signals were overwhelmed with EM noise.

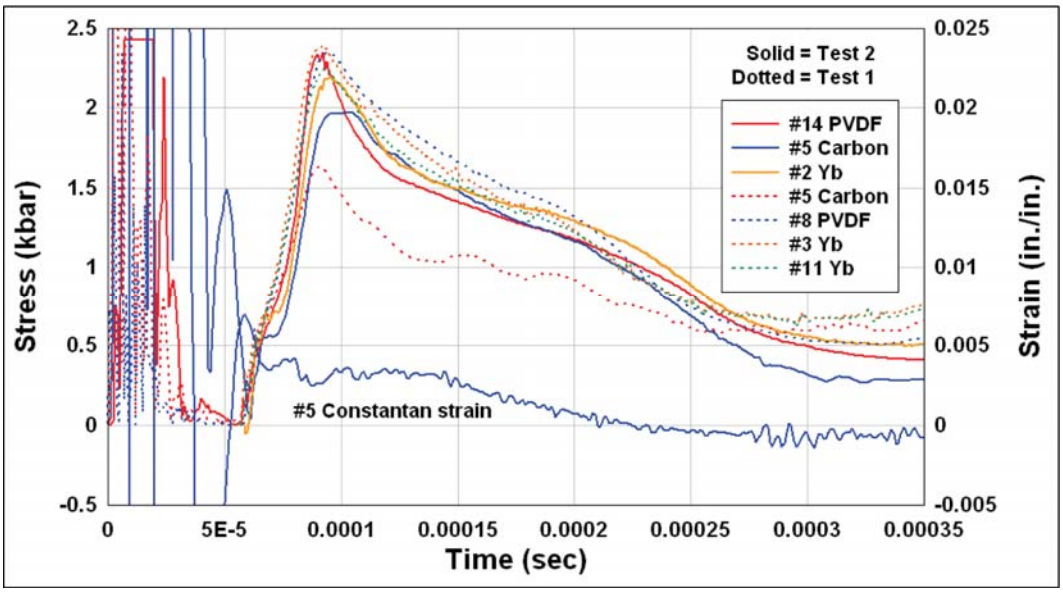

Figure 27. Test 1 and Test 2 flatpack stresses at the 9-in. radius.

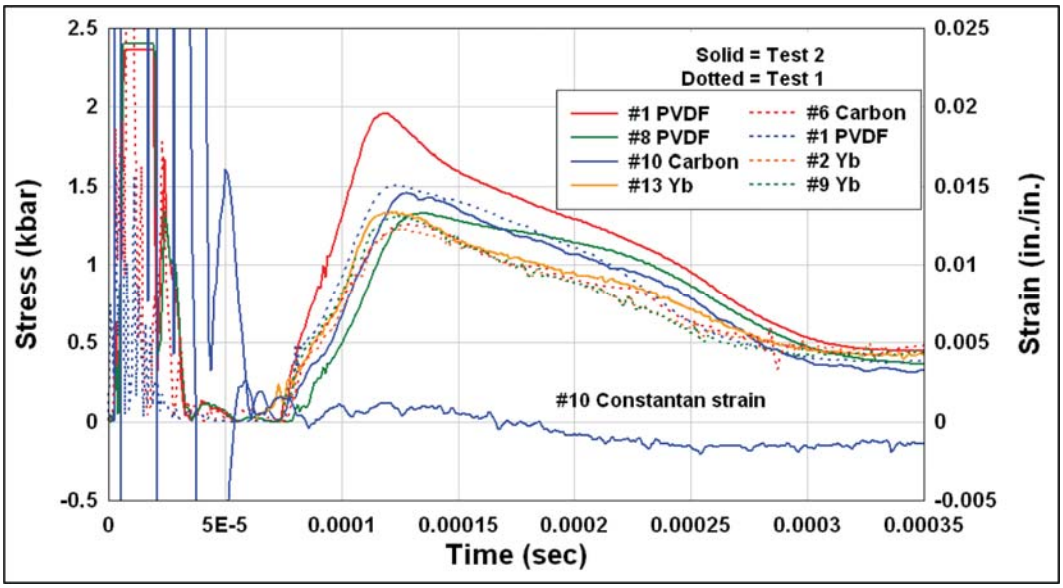

Figure 28. Test 1 and Test 2 flatpack stresses at the 12-in. radius.

The peak stresses from Tests 1 and 2 are plotted together and fit with a power-law function in Figure 29. The exponent of the fit is essentially identical to that for the archived data (see Figure 14).

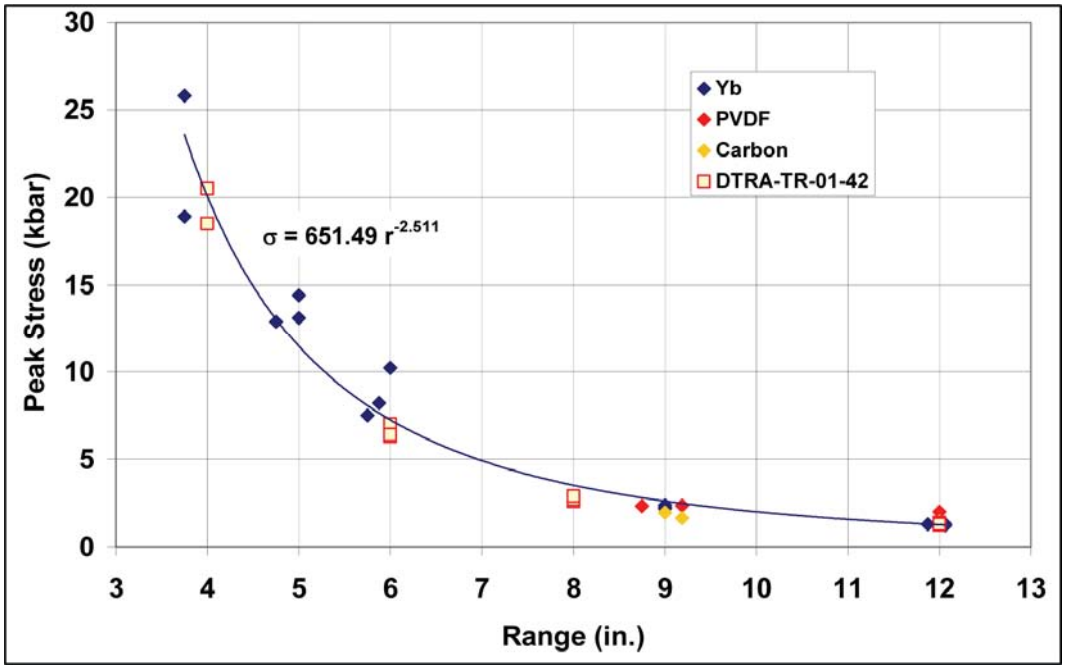

Figure 29. Test 1 and 2 peak stress attenuation.

Only one set of Dremin loops was used in Test 2 (DL16). The velocity records and their integrals (shown by the dashed lines) are plotted in Figure 30.

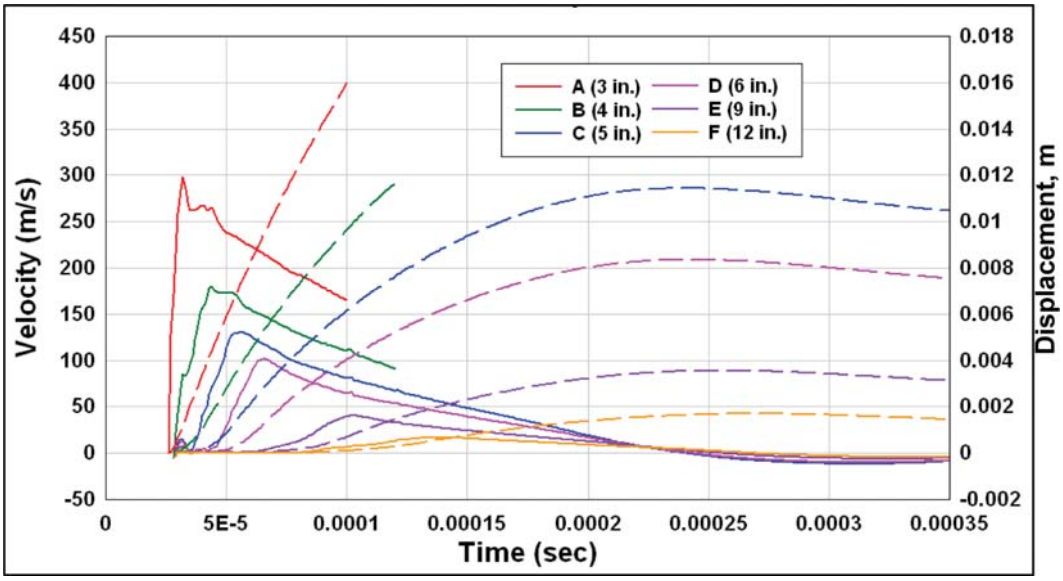

Figure 30. Test 2 Dremin loop radial velocity histories (DL16).

Figure 31 shows that the Test 2 Dremin loops recorded lower peak values and much longer rise times than the gages in Test 1. It appears that in Test 2 the stress wave in the quadrant of DL16 was perturbed by something very near the explosive charge, and the effect of that perturbation propagated out to all the other loops.

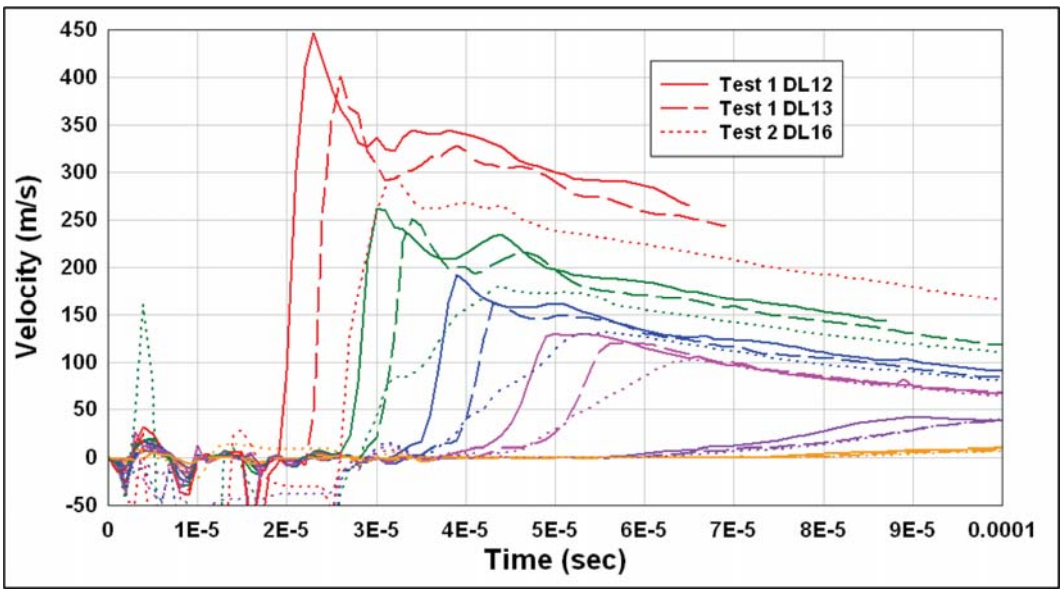

Figure 31. Test 1 and Test 2 Dremin loop records.

The displacements (integrals of velocity) from Test 2 are compared with the displacements from Test 1, in Figure 32. The Test 2 displacements clearly fall below those from Test 1 but much of the difference is due to the later times of arrival in Test 2. In fact, at ranges of 5 in. and greater, where long records are available for both tests, the peak displacements are about the same. Thus, the concrete circumferential strains at these ranges were also about the same in the two tests.

The times of first arrival for all the gages in Test 2 are plotted in Figure 33. The uncertainty in position is again set at ±1/8 in. For the flatpack, the uncertainty in TOA is again ±1 μs, but it is ±2 μs for the Dremin loops because of noise in the close-in gages and because of the less well defined toe in the outer gages. The straight line fits to both the stress and velocity data agree very well with the wave speeds observed in Test 1 (Figure 21). A distinct plastic wave front could not be detected in the Test 2 velocities.

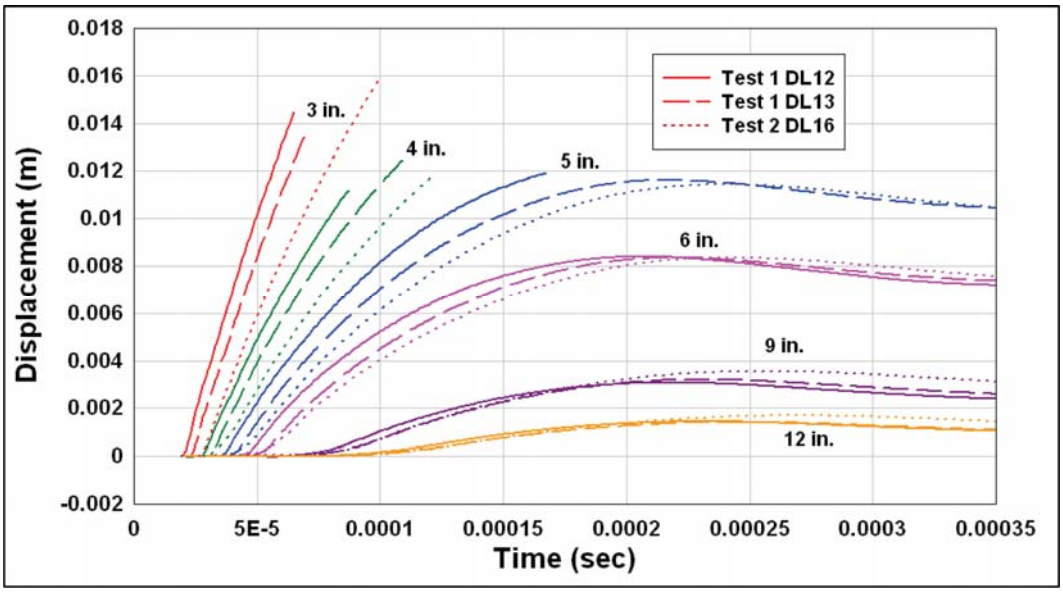

Figure 32. Test 1 and Test 2 Dremin loop displacement histories.

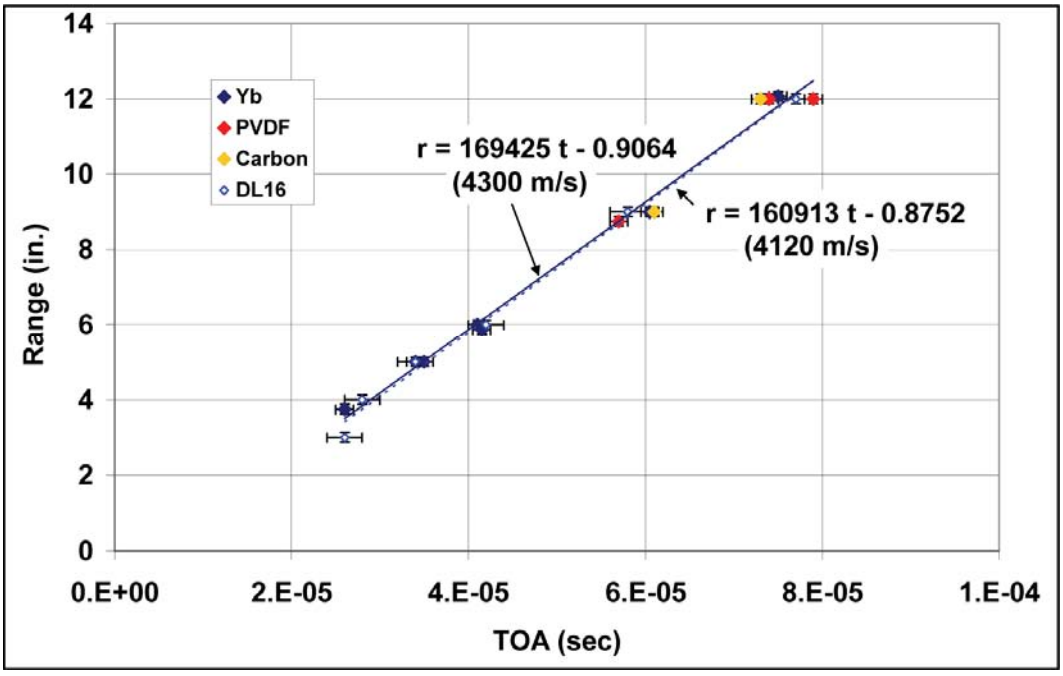

Figure 33. Test 2 times of arrival and wave velocities.

Test 3 results

The layout of the gages in Test 3 is shown in Figure 34, and the as-built locations of the gages are listed in Table 3. The locations of the Dremin loops are the range of the innermost loops. The charge depth is 18 in.

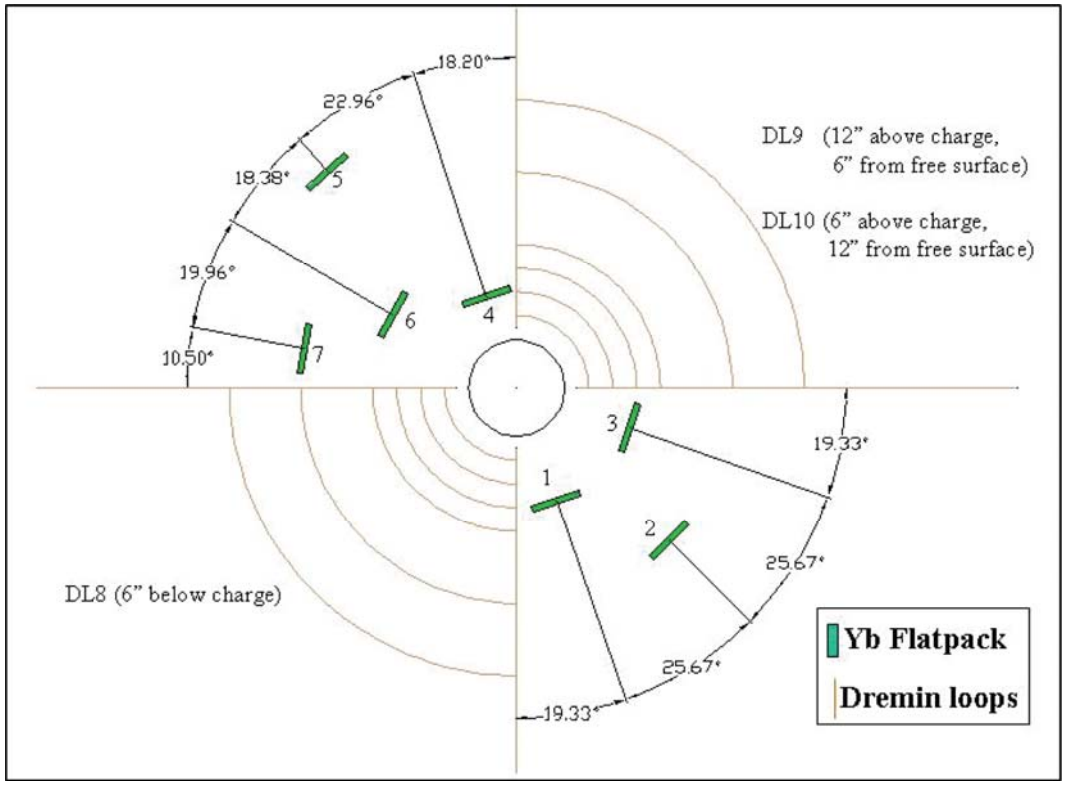

Figure 34. Test 3 gage layout (plan view).

Table 3. Test 3 as-built gage locations (±1/32 in.).

Ref #	Type	Radius	Depth
1	Yb FP	5.0625 in.	18 in.
2	Yb FP	8.9375 in.	18 in.
3	Yb FP	5 in.	18 in.
4	Yb FP	4 in.	18 in.
5	Yb FP	11.9375 in.	18 in.
6	Yb FP	6 in.	18 in.
7	Yb FP	9.0625 in.	18 in.
8	Dremin loops	3.25 in.	24 in.
9	Dremin loops	2.8 to 4.0 in.	6 in.
10	Dremin loops	3 in.	12 in.

The ytterbium flatpack stress measurements from Test 3 are shown in Figure 35, and the flatpack strains are shown in Figure 36. Because the charge in this test was closer to the free surface, reflections from the free surface reach the stress gages at about 220 μs (for an assumed wave speed of 4300 m/s), hence, peak stresses were not affected by reflections. The strains were comparable to those in Tests 1 and 2.

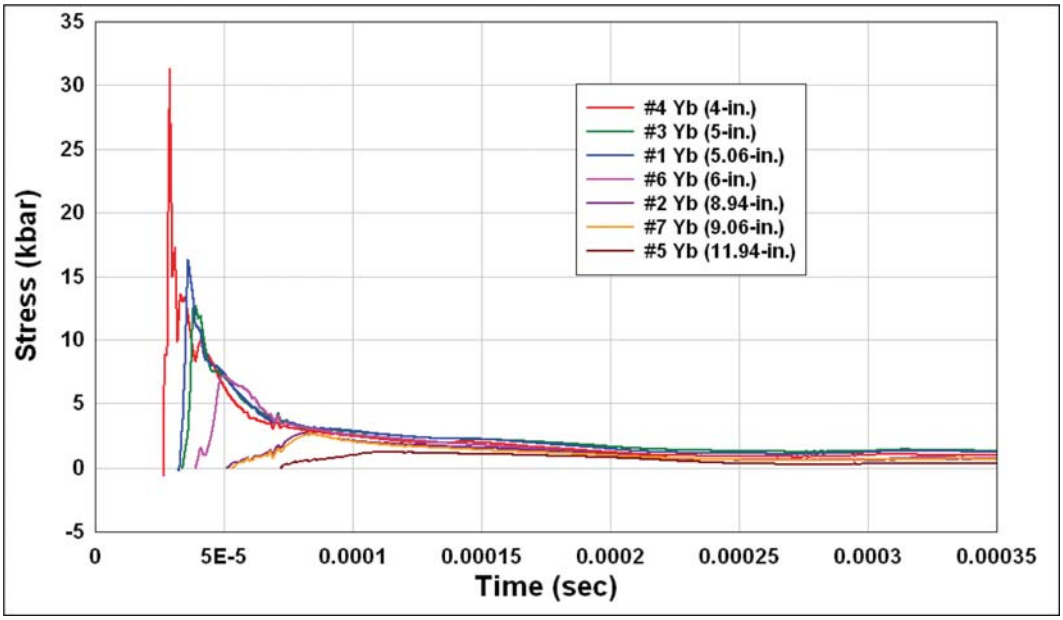

Figure 35. Test 3 ytterbium flatpack stresses.

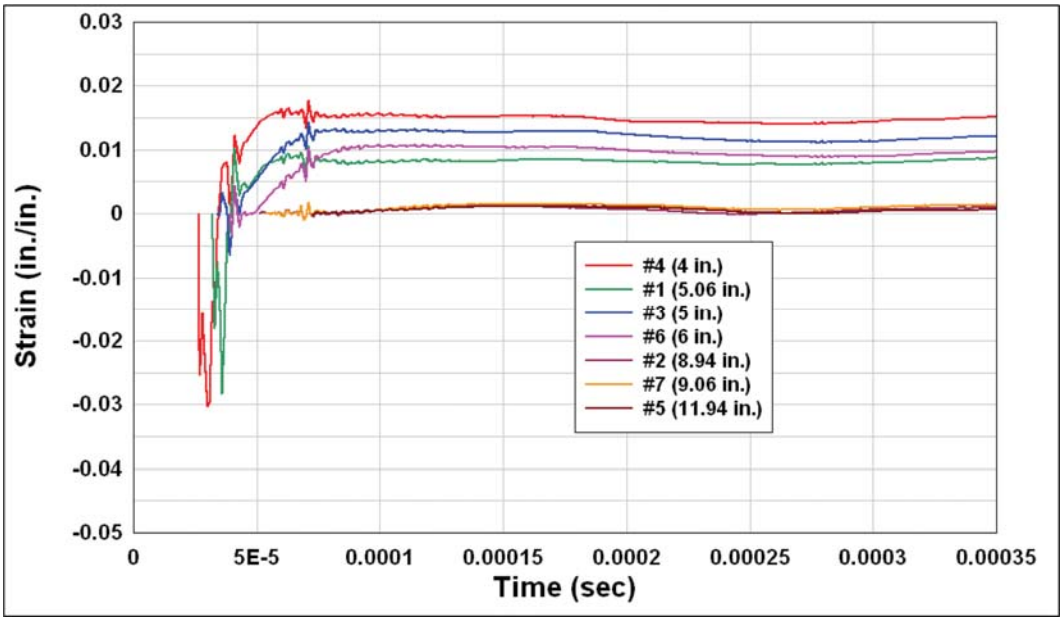

Figure 36. Test 3 ytterbium flatpack strains.

Comparisons of the ytterbium flatpack stresses from all three tests are shown in Figures 37 to 41, one plot for each gage range. In general, the agreement between the three tests is very good. Thus, it is reasonable to conclude that the outgoing stress wave in Test 3 was nominally the same as in Tests 1 and 2. At the 9- and 12-in. ranges, reflections from the free surface may be responsible for the lower stresses in Test 3 after 200 μs.

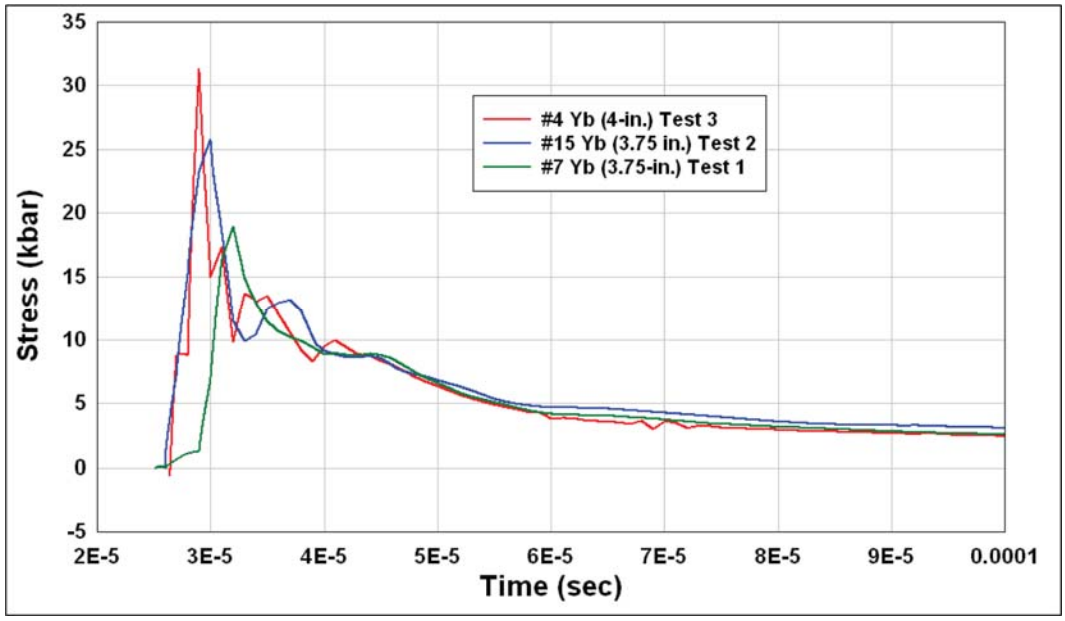

Figure 37. Test 1, 2, and 3 ytterbium flatpack stresses at the 4-in. range.

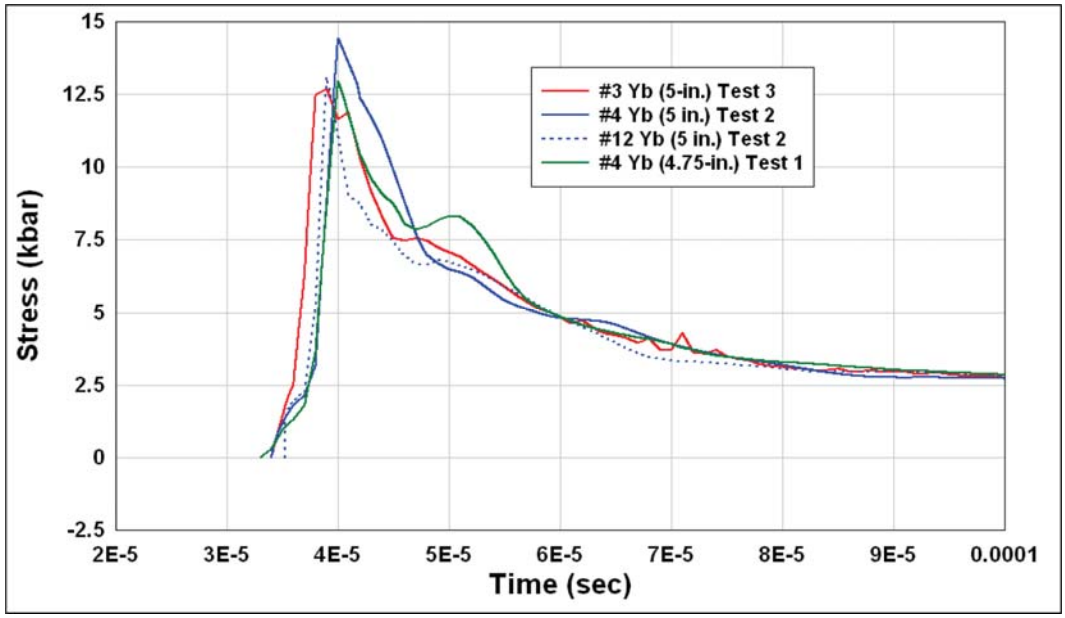

Figure 38. Test 1, 2, and 3 ytterbium flatpack stresses at the 5-in. range.

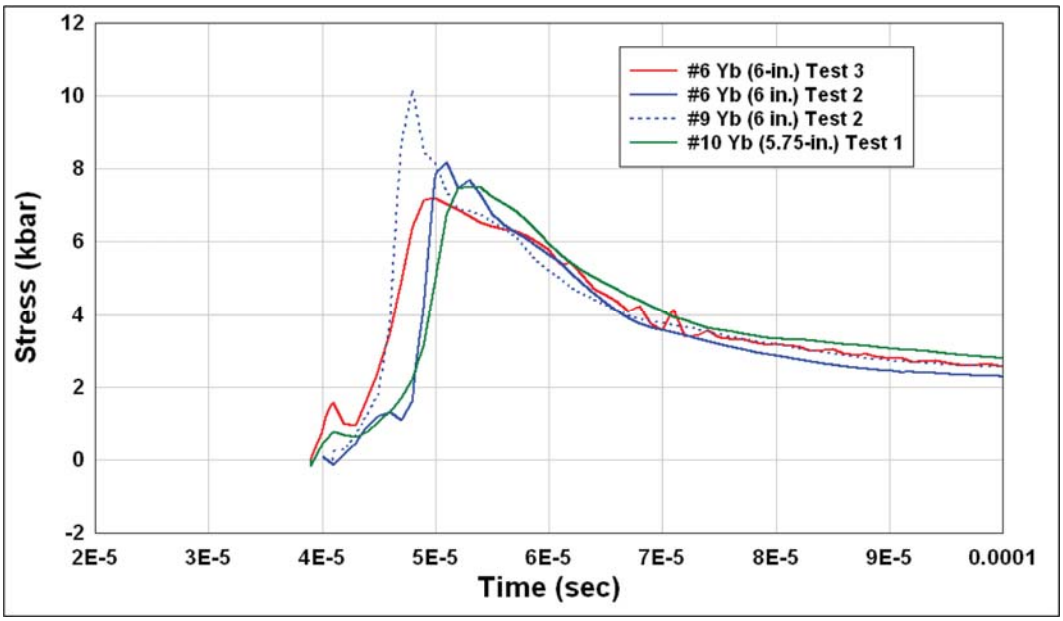

Figure 39. Test 1, 2, and 3 ytterbium flatpack stresses at the 6-in. range.

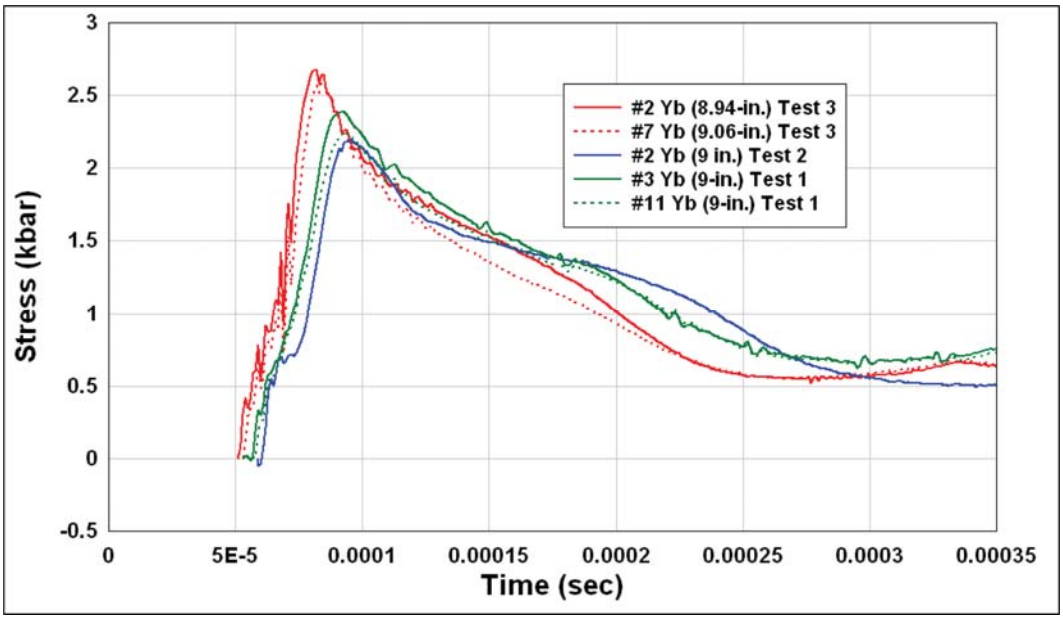

Figure 40. Test 1, 2, and 3 ytterbium flatpack stresses at the 9-in. range.

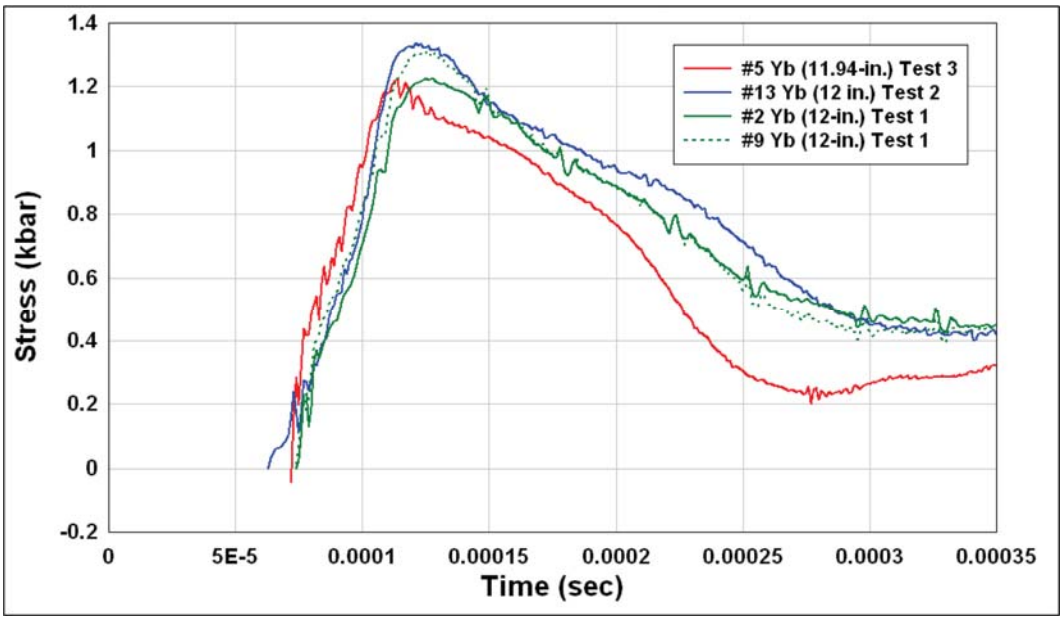

Figure 41. Test 1, 2, and 3 ytterbium flatpack stresses at the 12-in. range.

The peak stresses from all three tests are plotted in Figure 42 with a power-law fit to the entire set of measurements. The peaks from Test 3 are generally higher than those from Tests 1 and 2, especially at ranges of 6 in. or less. This raised the exponent in the power-law fit by a few percent (compare with Figure 29).

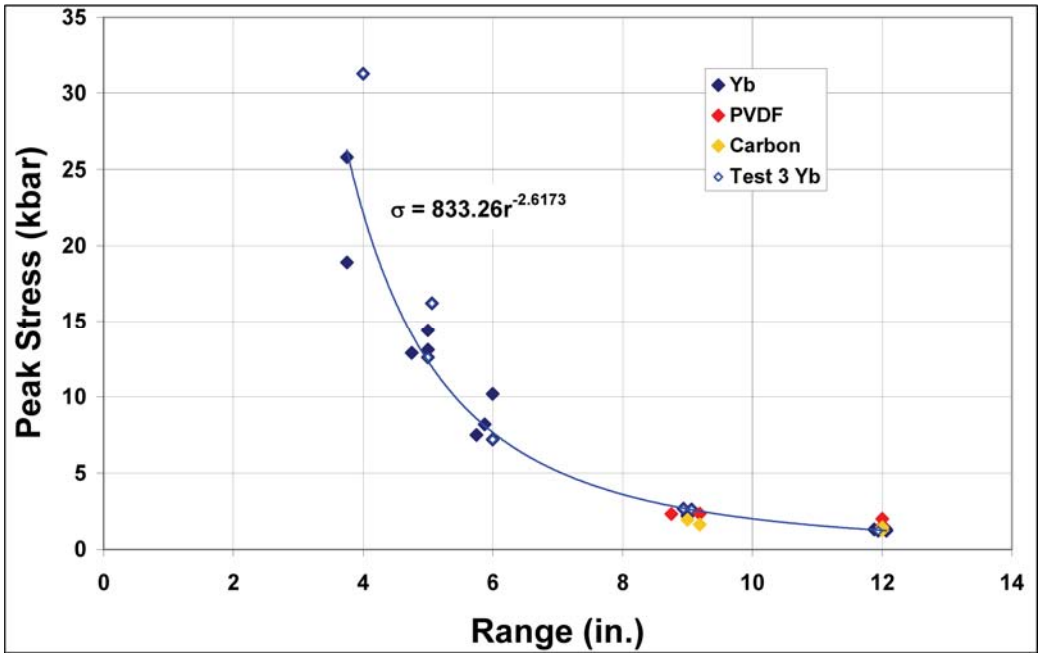

Figure 42. Peak stress attenuation in Tests 1, 2, and 3.

The Dremin loops in Test 3 were offset from the equatorial plane so that they measured the cylindrically radial velocity instead of the spherically radial velocity. The data from the Dremin loops arrays that were in planes ±6 in. from the charge equator (DL10 and DL8, respectively) are plotted together in Figure 43. Reflections from the free surface arrive at the DL8 gages at around 250 μs but they arrive at the DL10 gages at about 180 μs. The agreement is very good until the reflections arrive.

The Dremin loop velocities from DL9 (12 in. above the charge and only 6 in. from the free surface) are plotted in Figure 44. The reflections arrive at these gages at about 150 μs.

Even though the Dremin loops measured cylindrically radial velocity, the equivalent spherically radial velocity can be computed by dividing by the sine of the slant angle to the gage. If the flow was spherical, the peak spherical velocities obtained in this manner should agree with the peaks measured in Test 1. These spherical peaks are plotted in Figure 45. The plot shows that the peaks velocities from the Dremin loop arrays that were ±6 in. from the charge equator (DL10 and DL8) are consistent with the assumption of spherical flow. However, the peaks from the array that was 6 in. from the free surface (DL9) were affected by reflections except, possibly, the gages at the 9- and 12-in. radii.

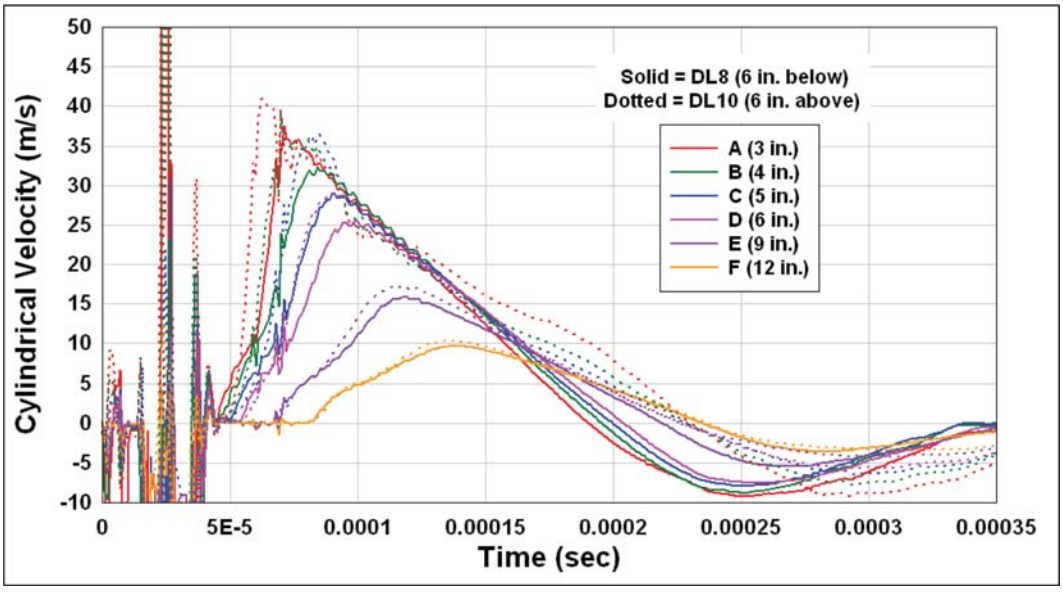

Figure 43. Test 3 Dremin loop velocities ±6 in. from the charge equator (DL10 and DL8).

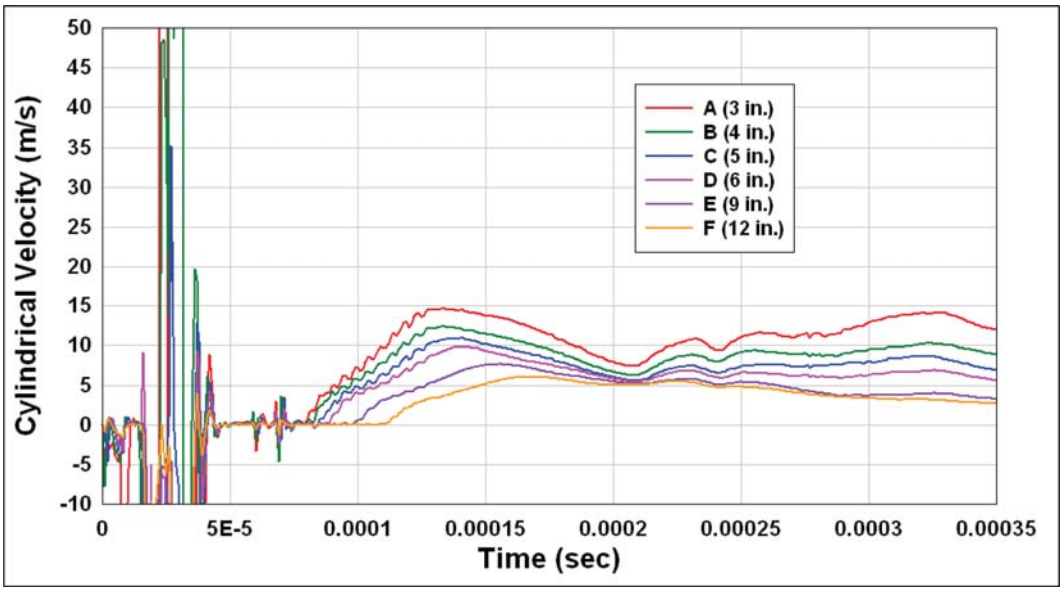

Figure 44. Test 3 Dremin loop velocities 12 in. above the charge equator (DL9).

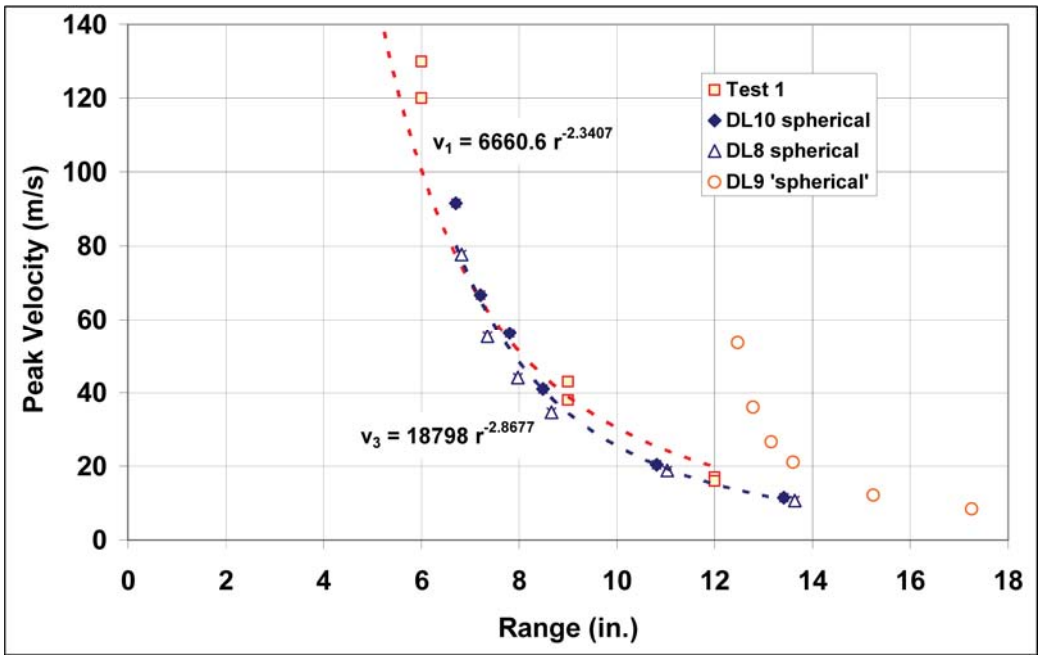

Figure 45. Sphericity of the peak Dremin loop velocities measured in Test 3.

Times of arrival for all the gages in Test 3 are plotted in Figure 46. The straight line fit though the TOAs at the flatpack stress gages indicates a wave velocity of over 4600 m/s, about 10% higher than observed in Tests 1 and 2. The Dremin loop TOAs indicate a wave speed of only about 4000 m/s. This fit may be overly weighted by the data from the DL9 gages at greater ranges than the ytterbium flatpacks. Note also that the uncertainty in the position of these loops is greater than for the others (see Table 3). The “plastic” wave arrival was taken from most of the Dremin

loop records, and these points are also plotted in Figure 46. The wave velocity that fits these points is about 3400 m/s, which is also higher than the plastic wave velocity in Test 1.

All the flatpack TOAs from Tests 1, 2, and 3 are plotted in Figure 47. The best fit to these data indicates a wave velocity of just under 4300 m/s.

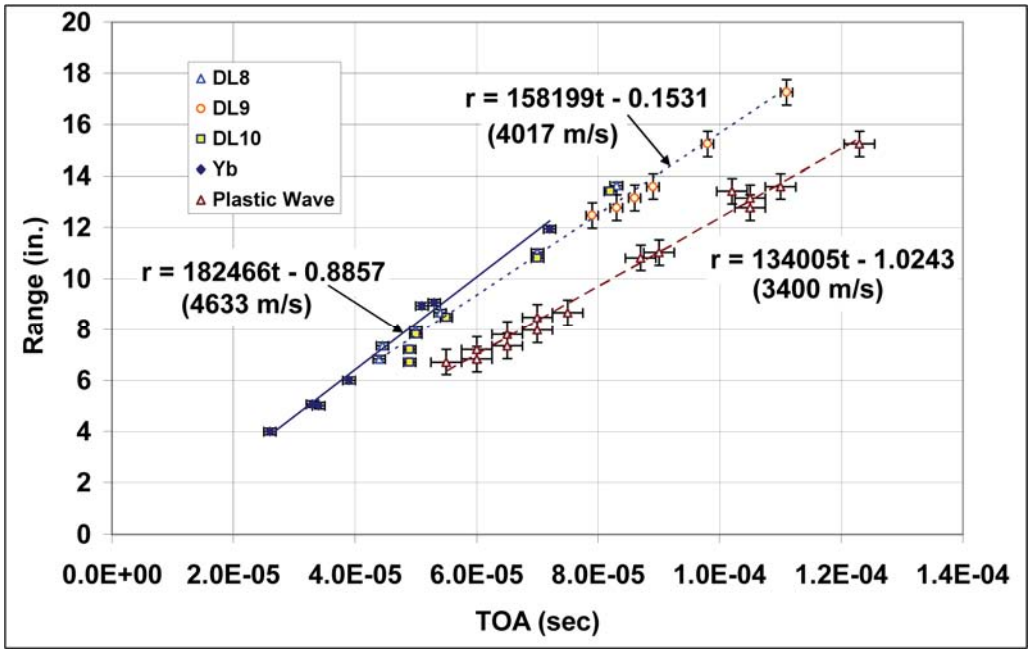

Figure 46. Test 3 times of arrival and wave velocities.

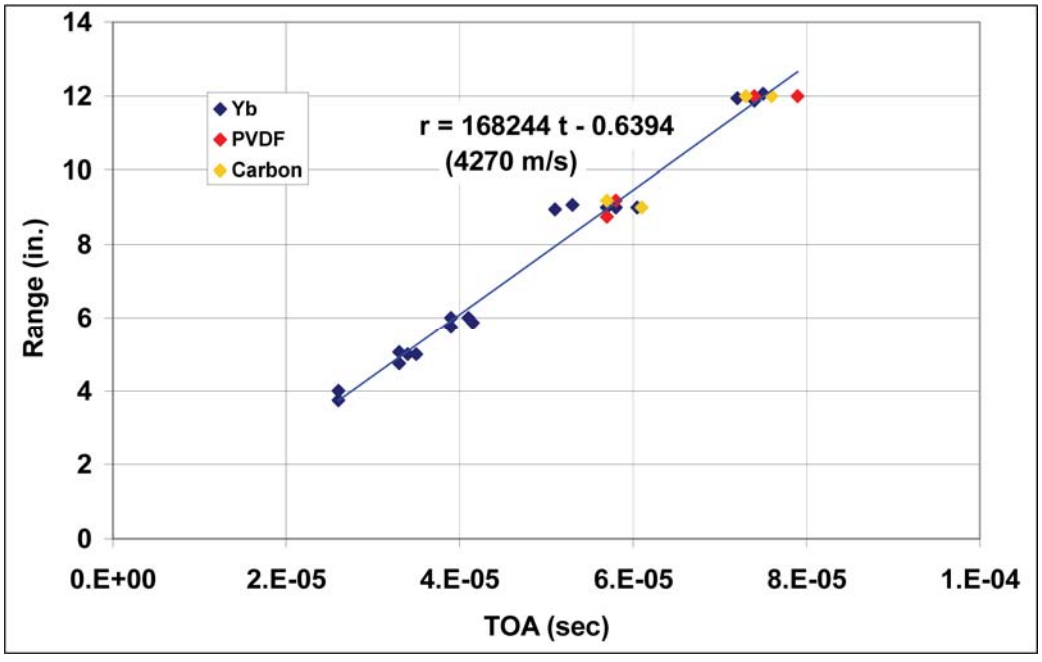

Figure 47. Times of arrival for all the flatpack stress gages in Tests 1, 2, and 3.

3 Conclusions and Recommendations

Conclusions

In general, these tests were very successful. All the ytterbium flatpack stress gages and all the Dremin loops functioned very well and provided excellent data. The results were very repeatable with the exception that the wave front measured by the Dremin loops in Test 2 appeared to have been dispersed very near the charge. The effect of the free surface near the charge in Test 3 was clearly captured in the velocity measurements. Thus, the data goals were accomplished.

In the spherical flow region of the targets, both the peak stress and peak velocity attenuated with range as $1/r^{2.6}$. Peak stresses and velocities varied by up to 25% from test to test, possibly due to target-to-target variations in the concrete or point-to-point variations. The bulk wave velocity was about 4300 m/s on average, and the plastic wave velocity was about 3200 m/s.

Electromagnetic noise at the time of explosive charge initiation infiltrated all the data records and created some difficulties in the data analysis, particularly in determining the first times of wave arrival at the close-in gages. It may also have introduced errors in the PIEZOR analysis for the ytterbium flatpack gages at the 3-in. radius.

The performance of carbon and PVDF flatpack gages was mixed. Most of them agreed fairly well with the ytterbium flatpacks at the same ranges, but there was more scatter and two clear outliers. Also, the data from one of the carbon flatpacks and from two of the PVDF flatpacks could not be used because of the electromagnetic noise.

Recommendations

Computational simulations should be performed to further interpret the data for material modeling purposes.

In future tests,

- the electromagnetic noise issue must be addressed and eliminated,
- redundant measurements are essential,
- more closely spaced gages should be used so that stress and displacement gradients in the radial direction can be resolved,
- ytterbium flatpacks should be used to measure circumferential stresses,
- longer duration velocity measurements at the close-in ranges should be attempted with annealed copper Dremin loops,
- carbon and PVDF should be tried at closer ranges to determine their limits of applicability.

References

Chen, D. Y., Y. M. Gupta, and M. H. Miles. 1984. Quasistatic experiments to determine material constants for piezoresistance foils used in shock wave experiments. *Journal of Applied Physics* 55(11).

Gran, J. K., and L. Seaman. 1997. Analysis of piezoresistance gages for stress in divergent flow fields. *Journal of Engineering Mechanics* 123(1).

Gran, J. K., R. E. Moxley, and M. D. Adley. 1999. Measurement of triaxial stresses during deep penetration into concrete. In *Proceedings, 9th International Symposium on the Effects of Munitions with Structures (ISIEMS), Strausberg, Germany*.

Gran, J. K., M. A. Groethe, and B. D. Peterson. 2004. *Subsystem precision tests.* SRI International FTR. DTRA-TR-01-42. Fort Belvoir, VA: Defense Threat Reduction Agency.

Rickman, D. D., J. Q. Ehrgott, Jr., J. K. Gran, S. A. Akers, and J. D. Cargile. 2006. Evaluation of lower-cost in-target stress measurements. *Proceedings, 19th International Symposium on Military Aspects of Blast and Shock (MABS 19), Calgary, Alberta, Canada*.

REPORT DOCUMENTATION PAGE

Form Approved
OMB No. 0704-0188

1. REPORT DATE *(DD-MM-YYYY)*	**2. REPORT TYPE**	**3. DATES COVERED** *(From - To)*
September 2009	Final report	

4. TITLE AND SUBTITLE

Cavity Expansion Experiments with Spherical Explosive Charges in Concrete

5a. CONTRACT NUMBER
W912HZ-08-P-0015

5b. GRANT NUMBER

5c. PROGRAM ELEMENT NUMBER

6. AUTHOR(S)

James K. Gran, John Q. Ehrgott, Jr., and J. Donald Cargile

5d. PROJECT NUMBER

5e. TASK NUMBER

5f. WORK UNIT NUMBER

7. PERFORMING ORGANIZATION NAME(S) AND ADDRESS(ES)

SRI International, 333 Ravenswood Avenue, Menlo Park, CA 94025;
U.S. Army Engineer Research and Development Center
Geotechnical and Structures Laboratory
3909 Halls Ferry Road, Vicksburg, MS 39180-6199

8. PERFORMING ORGANIZATION REPORT NUMBER

ERDC/GSL SR-09-4

9. SPONSORING / MONITORING AGENCY NAME(S) AND ADDRESS(ES)

Defense Threat Reduction Agency (DTRA/CXSS)
8725 John J. Kingman Road
Fort Belvoir, VA 22060-6201

10. SPONSOR/MONITOR'S ACRONYM(S)

11. SPONSOR/MONITOR'S REPORT NUMBER(S)

12. DISTRIBUTION / AVAILABILITY STATEMENT

Approved for public release; distribution is unlimited.

13. SUPPLEMENTARY NOTES

14. ABSTRACT

Three experiments were conducted with 1-lb explosive spheres embedded in large concrete cylinders with flatpack stress gages and Dremin loop velocity gages surrounding the charge. In two tests, the charge was far from the boundaries and was fully contained. Radial stresses and velocities attenuated with range by approximately $1/r^{2.5}$. In the third test, the charge was near the top surface of the concrete cylinder, and reflections perturbed the sphericity of the flow.

15. SUBJECT TERMS

Cavity expansion experiments
Concrete
Spherical explosive charge
Stress
Velocity

16. SECURITY CLASSIFICATION OF:			**17. LIMITATION OF ABSTRACT**	**18. NUMBER OF PAGES**	**19a. NAME OF RESPONSIBLE PERSON**
a. REPORT	**b. ABSTRACT**	**c. THIS PAGE**			**19b. TELEPHONE NUMBER** *(include area code)*
UNCLASSIFIED	UNCLASSIFIED	UNCLASSIFIED		52	